# Making corrections to your proof

Please follow these instructions to mark changes or add notes to your proof. Ensure that you have downloaded the most recent version of Acrobat Reader from **https://get.adobe.com** so you have access to the widest range of annotation tools.

The tools you need to use are contained in **Annotations** in the **Comment** toolbar. You can also right-click on the text for several options. The most useful tools have been highlighted here. If you cannot make the desired change with the tools, please insert a sticky note describing the correction.

Please ensure all changes are visible via the 'Comments List' in the annotated PDF so that your corrections are not missed.

Attach file
Highlight text
Insert sticky note
Insert text
Replace text
Strikethrough text
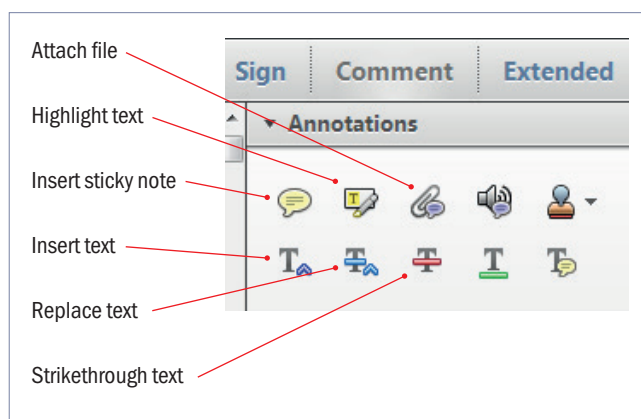
Do not attempt to directly edit the PDF file as changes will not be visible.

Replacing text

To replace text, highlight what you want to change then press the replace text icon, or right-click and press 'Add Note to Replace Text', then insert your text in the pop up box. Highlight the text and right click to style in bold, italic, superscript or subscript.
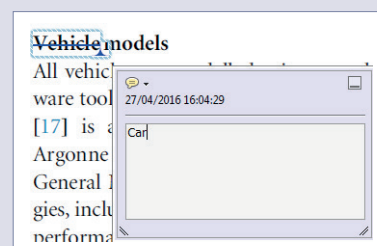
Inserting text

Place your cursor where you want to insert text, then press the insert text icon, or right-click and press 'Insert Text at Cursor', then insert your text in the pop up box. Highlight the text and right click to style in bold, italic, superscript or subscript.
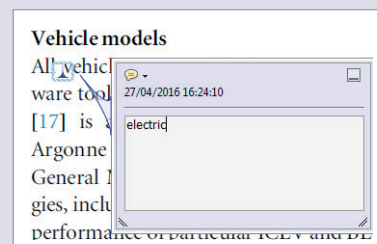
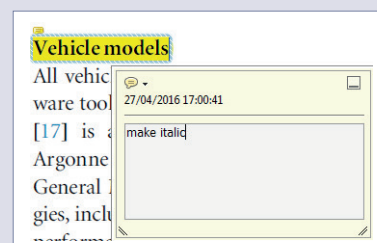### Deleting text

To delete text, highlight what you want to remove then press the strikethrough icon, or right-click and press 'Strikethrough Text'.
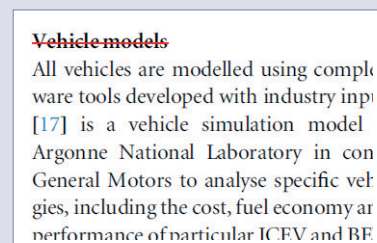
Highlighting text

To highlight text, with the cursor highlight the selected text then press the highlight text icon, or right-click and press 'Highlight text'. If you double click on this highlighted text you can add a comment.

QUERIES

Topical Review

100 years after Smoluchowski: stochastic processes in cell biology

D Holcman[1] and Z Schuss[2]

[1] Applied Mathematics and Computational Biology, Ecole Normale Supérieure, France and Churchill College, DAMTP Cambridge university, CB3 0DS, UK
[2] Department of Applied Mathematics, Tel-Aviv University, Tel-Aviv 69968, Israel

AQ1

E-mail: david.holcman@ens.fr

CrossMark

Abstract

100 years after Smoluchowski introduces his approach to stochastic processes, they are now at the basis of mathematical and physical modeling in cellular biology: they are used for example to analyse and to extract features from large number (tens of thousands) of single molecular trajectories or to study the diffusive motion of molecules, proteins or receptors. Stochastic modeling is a new step in large data analysis that serves extracting cell biology concepts. We review here the Smoluchowski's approach to stochastic processes and provide several applications for coarse-graining diffusion, studying polymer models for understanding nuclear organization and finally, we discuss the stochastic jump dynamics of telomeres across cell division and stochastic gene regulation.

Keywords: stochastic processes, biophysics, barrow escape, first passage time, polymer looping, stochatic gene activation, telomere modeling

AQ2

(Some figures may appear in colour only in the online journal)

1. Introduction

Stochastic processes have become the cornerstone of mathematical and physical modeling in cellular biology. Their role is to simulate and predict measurable cellular biology phenomena from molecular level physics. The early theory began with Einstein's early work on the Brownian motion in configuration space [1], which was extended by Langevin [2] to the stochastic description of Brownian motion in phase space. A major advancement was Smoluchowski's observation [3] that in the overdamped regime of Langevin's phase space-model, displacement and velocity become statistically independent and thus the analysis of the Langevin model reduces to that of displacement in configuration space alone, while velocities remain Maxwellian. This reduction made the use of the Fokker–Planck–Smoluchowski–Kolmogorov

partial differential equations the main tool for extracting probabilistic and thus physical and chemical information from molecular models. In particular, the solution of boundary value problems for these partial differential equations clarified the significance of the mean escape time of a Smoluchowski configuration-space trajectory from the domain of attraction of a stable attractor, such as the escape over a potential barrier, called thermal activation. Chandrasekhar's 1943 paper [11] reviews the early period of stochastic models in different branches of physics, chemistry and astronomy. In particular, it reviews Kramers' theory [12] of thermal activation over a potential barrier and his development of an asymptotic method for the approximation of the solution of singular perturbation problems for the Fokker–Planck–Smoluchowski partial differential equation. Kramers' theory was developed further in the 1950s–2000s and applied in many physical, chemical, and engineering problems, such as impurity diffusion in crystals, the transitions between super-conducting and conducting states of the driven Josephson junction, loss of lock in tracking loops, and other non-equilibrium processes [16, 18].

In the early 1970s a new direction has emerged. Merton, Black, and Scholes developed a Smoluchowski-type stochastic model for the market value of stock and used it to predict the value of a future contract on the stock, given its current market value (stock option pricing theory), for which they were awarded the 1997 Nobel Prize in economics. Since the publication of their paper in 1973 the market of stock derivatives exploded and the value of traded derivatives became significantly bigger than all commodities put together, including real estate in downtown Tokyo.

Following the work of Einstein, Langevin, and Smoluchowski a partial differential equation was derived by Fokker in 1914 (for a linear model) and in 1917 by Planck for the general Langevin equation (see [11, 18] for references). The rigorous mathematical treatment of the relationship between Langevin trajectories and partial differential equations began in the 1930s with the formalism of Kolmogorov and Wiener, who put it into abstract probability theory. In the mathematical literature it became clear that in addition to Itô's formulation, which assumed that the noise and the state are independent, there is another formulation, due to Stratonovich, that takes into account correlations between the state and the noise. This is important both in modeling and simulations. The question which form, Itô or Stratonovich, is correct for the given model, is answered at the microscopic level, not at the equation level (see discussion in [18]).

The calculation of the mean first passage time (MFPT) for noise-activated escape from the an attractor leads to singular perturbation problems in parabolic and elliptic partial differential equations. Therefore analytical approximations of the solution require asymptotic methods that were developed in fluid dynamics [5] and quantum mechanics [6, 7], such as boundary layer theory [7, 8], matched asymptotics [9], the WKB method [7, 8, 10], and more.

Molecular and cellular biophysics were relatively late comers to the world of stochastics. They introduced a slew of new mathematical problems in stochastics. Thus, for instance, Smoluchowski and Smoluchowski–Stratonovich equations appear as approximations to Markovian models in the continuum limit. Deviations from the Smoluchowski–Stratonovich model are expressed by the introduction of a memory kernel, which may represent a coarse-grained model of interaction of the molecular path with many degrees of freedom, such as the medium in which a molecule is immersed, coupling between molecules, and so on [18].

In the 1980s and 1990s, motivated by biophysical questions, modeling and simulations were developed to simulate and analyze the motion of ions inside protein channels of biological membranes or across different concentrations [33, 34]. Later, in the 1990s and the 2000s, a new field emerged that used Smoluchowski dynamics to predict biological processes on the molecular level. Specifically, the accumulation of massive physiological data prompted the

use of stochastic models of synaptic transmission in neurobiology, of calcium dynamics in microdomains, the motion of ions in selective ion channels, and so. The narrow escape theory emerged as a generic theory to study the rare cellular events of arrival of Brownian particles at a small absorbing part of an impermeable membrane, which may represent any small target for diffusing molecules [14, 35–42, 44, 45].

Nowadays, 100 years after Smoluchowski, the field of stochastic modeling has matured into molecular biophysics and physiology and brought with it a plethora of new mathematical problems. A particularly fruitful direction is that of calculating the MFPT of a Smoluchowski trajectory to a small target, the so-called narrow escape problem. Obviously, the Smoluchowski trajectory may represent that of a molecule inside or outside a biological cell or on its membrane. The target is small in the sense that its size is much smaller than that of the cell. Although similar to the activation problem, the narrow escape problem is radically different and calls for new asymptotic methods. Curiously enough, the same mathematical problem appears in Helmholtz's theory of radiation through a small opening [46]. The new narrow escape theory (NET), which appeared initially as a new mathematical first passage time problem, is the centerpiece of this review.

2. Construction of the Brownian trajectories

The laws of diffusion were first formulated by Fick. His first law of diffusion, formulated in 1856 by analogy with Fourier's first law of heat conduction, asserts that *the diffusion flux between two points of different concentrations in the fluid is proportional to the concentration gradient between these points*. The constant of proportionality is called *the diffusion coefficient* and it is measured in units of area per unit time.

In 1905 Einstein [1] and, independently, in 1906 Smoluchowski [3] offered an explanation of the Brownian motion based on kinetic theory and demonstrated, theoretically, that the phenomenon of diffusion is the result of Brownian motion. Einstein's theory was later verified experimentally by Perrin [21] and Svedberg [22]. That of Smoluchowski was verified by Smoluchowski [4], Svedberg [23] and Westgren [24, 25]. Perrin has won the 1926 Physics Nobel Prize for his experiment.

They derived an explicit formula for the diffusion coefficient,

$$D = \frac{RT}{N} \frac{1}{6\pi a\eta}, \tag{1}$$

where R is the universal gas constant, T = absolute (Kelvin) temperature, and N = Avogadro's number, a = radius of the particle, and η = coefficient of dynamical viscosity. Equation (1) was obtained from similar considerations by Sutherland in 1904 and published in 1905 [26], but has never received due credit for it.

To connect this theory with the ' *irregular movement which arises from thermal molecular movement*', Einstein made the following assumptions: *(1) the motion of each particle is independent of the others and (2) 'the movements of one and the same particle after different intervals of time must be considered as mutually independent processes, so long as we think of these intervals of time as being chosen not too small'*. He derived from these assumptions the diffusion equation for the density function $p(x,t)$ of finding the Brownian particle at point x on the line at time t and its solution

$$p(x, t) = \frac{1}{\sqrt{4\pi Dt}} \exp\left\{-\frac{x^2}{4Dt}\right\}, \tag{2}$$

which can be interpreted as the transition probability density of a particle from the point $x = 0$ at time 0 to the point x at time t.

If we denote by $x(t)$ the displacement (or trajectory) of the particle at time t, then for any spatial interval A,

$$\Pr\{x(t) \in A\} = \int_A p(x, t)\, \mathrm{d}x. \tag{3}$$

It follows that the moments of the Brownian displacement process are

$$\mathbb{E}x(t) = \int xp(x, t)\, \mathrm{d}x = \mathbb{E}x(t) = 0, \quad \mathbb{E}x^2(t) = 2Dt. \tag{4}$$

Obviously, if the particle starts at $x(0) = x_0$, then

$$\begin{aligned}
\mathbb{E}[x(t) \mid x(0) = x_0] &= x_0 \\
\mathrm{Var}[x(t) \mid x(0) = x_0] &= \mathbb{E}[(x(t) - x_0)^2 \mid x(0) = x_0] = 2Dt.
\end{aligned} \tag{5}$$

Now, using equation (1) in equation (5), the mean square displacement of a Brownian particle along the x-axis is found as

$$\sigma = \sqrt{t}\sqrt{\frac{kT}{3\pi a\eta}}, \tag{6}$$

where $k = R/N$ is Boltzmann's constant. This formula was verified experimentally [22]. It indicates that the mean square displacement of a Brownian particle at times t not too short is proportional to the square root of time.

The mathematical question of the existence of a stochastic (random) process which satisfies Einstein's requirements and of its actual construction, was answered in the affirmative in 1933 by Paley, Wiener, and Zygmund [27], who constructed the random Brownian trajectories in the form of a Fourier series with random Gaussian coefficients. They proved, i.e. that the Brownian trajectories are nowhere differentiable with probability 1. Another, more modern approach, was proposed by Lévy [28]. Lévy's construction of a Brownian path in the time interval [0,1] consist in refining linear interpolations of points sampled independently from the Gaussian distribution at binary times $t_{k,n} = k2^{-n}$, $(k = 0, 1 \ldots, n)$, such that the properties (4), (5) are satisfied at the binary times $t_{k,n}$ (see details in [18]).

3. The velocity process and Langevin's approach

3.1. The velocity problem

Obviously, the infinite velocities of the Brownian trajectories contradict physics. Specifically, according to the Waterston–Maxwell equipartition theorem [20], the root mean square (RMS) velocity $\bar{v} = \sqrt{\mathbb{E}v^2}$ of a suspended particle should be determined by the equation

$$\frac{m}{2}\bar{v}^2 = \frac{3kT}{2}. \tag{7}$$

Each component of the velocity vector has the same variance, so that

$$\frac{m}{2}\bar{v}^2_{x,y,z} = \frac{kT}{2}, \tag{8}$$

which is the one-dimensional version of equation (7). The RMS velocity comes out to be about $8.6 \, \mathrm{cm \, s^{-1}}$ for the particles used in Svedberg's experiment [22]. Einstein argued in 1907 and 1908 [1] that there is no possibility of observing this velocity, because of the very rapid viscous damping, which can be calculated from the Stokes formula. The velocity of such a particle would drop to 1/10 of its initial value in about 3.3×10^{-7} s. Therefore, Einstein argued, in the period τ between observations the particle must get new impulses to movement by some process that is the inverse of viscosity, so that it retains a velocity whose RMS average is $\bar{v}$. Between consecutive observations these impulses alter the magnitude and direction of the velocity in an irregular manner, even in the extraordinarily short time of 3.3×10^{-7} s. According to this theory, the RMS velocity in the interval τ has to be inversely proportional to $\sqrt{\tau}$; that is, it increases without limit as the time interval between observations becomes smaller.

3.2. Langevin's solution of the velocity problem

In 1908 Langevin [2] offered an alternative approach to the problem of the Brownian motion. He assumed that the dynamics of a free Brownian particle is governed by the frictional force $-6\pi a \eta v$ and by a fluctuational force Ξ that results from the random collisions of the Brownian particle with the molecules of the surrounding fluid, after the frictional force is subtracted. This force is random and assumes positive and negative values with equal probabilities. It follows that Newton's second law of motion for the Brownian particle is given by

$$m\ddot{x} = -6\pi a \eta \dot{x} + \Xi. \tag{9}$$

Denoting $v = \dot{x}$ and multiplying equation (9) by x, we obtain

$$\frac{m}{2}\frac{\mathrm{d}^2}{\mathrm{d}t^2}x^2 - mv^2 = -3\pi a \eta \frac{\mathrm{d}}{\mathrm{d}t}x^2 + \Xi x. \tag{10}$$

Averaging under the assumption that the fluctuational force Ξ and the displacement of the particle x are independent, we obtain

$$\frac{m}{2}\frac{\mathrm{d}^2}{\mathrm{d}t^2}\mathbb{E}x^2 + 3\pi a \eta \frac{\mathrm{d}}{\mathrm{d}t}\mathbb{E}x^2 = kT, \tag{11}$$

where (8) has been used. The solution is given by $\mathrm{d}\mathbb{E}x^2/\mathrm{d}t = kT/3\pi a \eta + C\mathrm{e}^{-6\pi a \eta t/m}$, where C is a constant. The time constant in the exponent is 10^{-8} sec, so the mean square speed decays on a time scale much shorter than that of observations. It follows that $\mathbb{E}x^2 - \mathbb{E}x_0^2 = (kT/3\pi a \eta)t$. This, in turn (see (4)), implies that the diffusion coefficient is given by $D = kT/6\pi a \eta$, as in Einstein's equation (1).

Langevin's equation (9) is a *stochastic differential equation*, because it is driven by a random force Ξ. If additional fields of force act on the diffusing particles (e.g. electrostatic, magnetic, gravitational, etc), Langevin's equation is modified to include the external force, $F(x,t)$, say, [12], [11],

$$m\ddot{x} + \Gamma\dot{x} - F(x,t) = \Xi, \tag{12}$$

where $\Gamma = 6\pi a \eta$ is the friction coefficient of a diffusing particle. We denote the dynamical friction coefficient (per unit mass) $\gamma = \Gamma/m$. If the force can be derived from a potential, $F = -\nabla U(x)$, Langevin's equation takes the form

$$m\ddot{x} + \Gamma\dot{x} + \nabla U(x) = \Xi. \tag{13}$$

The main mathematical difference between the two approaches is that Einstein assumes that the displacements Δ are independent, whereas Langevin assumes that the random force Ξ and the displacement x are independent. The two theories are reconciled in section 3.3 below.

To investigate the statistical properties of the fluctuating force Ξ, Langevin made the following assumptions.

 (i) *The fluctuating force Ξ is independent of the velocity v.*
 (ii) *Ξ changes much faster than v.*
(iii) $\langle \Xi \rangle = 0$.
(iv) *The accelerations imparted in disjoint time intervals Δt_1 and Δt_2 are independent.*

These conditions define the noise $\Xi(t)$ (so called *white noise*) as the nonexistent derivative of Einstein's Brownian motion $X(t)$. The conditional probability distribution function of the velocity process of a Brownian particle (PDF), given that it started with velocity v_0 at time $t = 0$, is defined as $P(v, t \mid v_0) = \Pr\{v(t) < v \mid v_0\}$ and the conditional probability density function is defined by

$$p\,(v, t \mid v_0) = \frac{\partial P(v, t \mid v_0)}{\partial v}.$$

In higher dimensions, we denote the displacement vector $\boldsymbol{x} = (x_1, x_2, \ldots, x_d)^T$, the velocity vector $\dot{\boldsymbol{x}} = \boldsymbol{v} = (v_1, v_2, \ldots, v_d)^T$, the random force vector $\boldsymbol{\Xi} = (\Xi_1, \Xi_2, \ldots, \Xi_d)^T$, the PDF

$$P(\boldsymbol{v}, t \mid \boldsymbol{v}_0) = \Pr\{v_1(t) < v_1, v_2(t) < v_2, \ldots, v_d(t) < v_d \mid \boldsymbol{v}(0) = \boldsymbol{v}_0\},$$

and the probability density function (pdf)

$$p\,(\boldsymbol{v}, t \mid \boldsymbol{v}_0) = \frac{\partial^n P(\boldsymbol{v}, t \mid \boldsymbol{v}_0)}{\partial v_1 \partial v_2, \ldots \partial v_d}.$$

The conditioning implies that the initial condition for the pdf is $p\,(\boldsymbol{v}, t \mid \boldsymbol{v}_0) \to \delta(\boldsymbol{v} - \boldsymbol{v}_0)$ as $t \to 0$. According to the Waterston–Maxwell theory, when the system is in thermal equilibrium, the velocities of free Brownian particles have the Maxwell–Boltzmann pdf; that is,

$$\lim_{t \to \infty} p\,(\boldsymbol{v}, t \mid \boldsymbol{v}_0) = \left(\frac{m}{2\pi kT}\right)^{3/2} \exp\left\{-\frac{m|\boldsymbol{v}|^2}{2kT}\right\}. \tag{14}$$

The solution of the Langevin equation (9) for a free Brownian particle is given by

$$\boldsymbol{v}(t) = \boldsymbol{v}_0 \mathrm{e}^{-\gamma t} + \frac{1}{m}\int_0^t \mathrm{e}^{-\gamma(t-s)} \boldsymbol{\Xi}(s)\,\mathrm{d}s. \tag{15}$$

The integral (15) makes sense, if it is integrated once by parts. However, if the factor multiplying Ξ in (15) is non-differentiable as well, e.g. if it is $\boldsymbol{x}(t)$, integration by parts is insufficient to make sense of the stochastic integral and a more sophisticated definition is needed. Such a definition was given by Itô in 1944 [29] (see also [18]).

To interpret the stochastic integral in the one-dimensional (15), we make a short mathematical digression on the definition of integrals of the type $\int_0^t g(s)\Xi(s)\,\mathrm{d}s$, where $g(s)$ is a deterministic integrable function. Such an integral is defined as the limit of finite Riemann sums of the form

$$\int_0^t g(s)\Xi(s)\,\mathrm{d}s = \lim_{\Delta s_i \to 0} \sum_i g(s_i)\Xi(s_i)\,\Delta s_i, \tag{16}$$

where $0 = s_0 < s_1 < \cdots < s_N = t$ is a partition of the interval $[0,t]$. According to the assumptions about Ξ, if we choose $\Delta s_i = \Delta t = t/N$ for all i, the Gaussian increments $\Delta b_i = \Xi(s_i)\,\Delta s_i$ are independent identically distributed (i.i.d.) random variables. Einstein's observation (see the beginning of section 3) that the RMS velocity on time intervals of length Δt are inversely proportional to $\sqrt{\Delta t}$, implies that if the increments $b_i = \Xi(s_i)\,\Delta s_i$ are chosen to be normally distributed, their mean must be zero and their covariance matrix must be $\langle \Delta b_i \Delta b_j \rangle = q\Delta t \delta_{ij}$ with q a parameter to be determined. We write $\Delta b_i \sim \mathcal{N}(0, q\Delta t)$. Then $g(s_i)\Xi(s_i)\,\Delta s_i \sim \mathcal{N}(0, |g(s_i)|^2 q\Delta t)$, so that $\sum_i g(s_i)\Xi(s_i)\,\Delta s_i \sim \mathcal{N}(0, \sigma_N^2)$, where $\sigma_N^2 = \sum_i |g(s_i)|^2 q\Delta s_i$. As $\Delta t \to 0$, we obtain $\lim_{\Delta t \to 0} \sigma_N^2 = q\int_0^t g^2(s)\,\mathrm{d}s$ and $\int_0^t g(s)\Xi(s)\,\mathrm{d}s \sim \mathcal{N}(0, \sigma^2)$, where

$$\sigma^2 = q \int_0^t g^2(s)\,\mathrm{d}s. \tag{17}$$

To interpret (15), we use (17) with $g(s) = \mathrm{e}^{-\gamma(t-s)}$ and obtain

$$\sigma^2 = \frac{q}{2\gamma}(1 - \mathrm{e}^{-2\gamma t}). \tag{18}$$

Returning to the velocity vector $\boldsymbol{v}(t)$, we obtain from the above considerations

$$\boldsymbol{v}(t) - \boldsymbol{v}_0 \mathrm{e}^{-\gamma t} \sim \mathcal{N}(\boldsymbol{0}, \sigma^2 \boldsymbol{I}) \tag{19}$$

with σ^2 given by (18). Finally, the condition (14) implies that $q = 2\gamma kT/m$, so that in 3D the mean energy is as given in equation (7). Itô's construction of the stochastic integral allows $g(t)$ to be stochastic, but independent of the Brownian increments $\Xi(s_i)\Delta s_i = X(s_i + \Delta s_i) - X(s_i)$.

In the limit $\gamma \to \infty$ the acceleration $\gamma\boldsymbol{v}(t)$ inherits the properties of the random acceleration $\Xi(t)$ in the sense that for different times $t_2 > t_1 > 0$ the accelerations $\gamma\boldsymbol{v}(t_1)$ and $\gamma\boldsymbol{v}(t_2)$ become independent. In fact, from equations (15) and $\Delta b_i \sim \mathcal{N}(0, q\Delta t)$, we find that

$$\lim_{\gamma \to \infty} \mathbb{E}[\gamma\boldsymbol{v}(t_1) \cdot \gamma\boldsymbol{v}(t_2)] = 0$$

and a similar result for $0 < t_2 < t_1$. It follows that for $\gamma(t_1 \wedge t_2) \gg 1$,

$$\mathbb{E}[\gamma\boldsymbol{v}(t_1) \cdot \gamma\boldsymbol{v}(t_2)] = \frac{\gamma q}{m^2}\mathrm{e}^{-\gamma|t_2 - t_1|}(1 + o(1)) = \frac{2q}{m^2}\delta(t_2 - t_1)(1 + o(1)), \tag{20}$$

because for $t_1 > 0$

$$\lim_{\gamma \to \infty} \int_0^\infty f(t_2)\frac{\gamma}{m^2}\mathrm{e}^{-\gamma|t_2 - t_1|}(1 + o(1))\,\mathrm{d}t_2 = \frac{2}{m^2}f(t_1) \tag{21}$$

for all test functions $f(t)$ in $\mathbb{R}^+$.

3.3. The displacement process

The displacement of a free Brownian particle is obtained from integration of the velocity process,

$$\boldsymbol{x}(t) = \boldsymbol{x}_0 + \int_0^t \boldsymbol{v}(s)\,\mathrm{d}s. \tag{22}$$

Using the expression (15) in equation (22) and changing the order of integration in the resulting iterated integral, we obtain

$$\boldsymbol{x}(t) - \boldsymbol{x}_0 - \boldsymbol{v}_0 \frac{1 - e^{-\gamma t}}{\gamma} = \int_0^t g(s) \boldsymbol{\Xi}(s) \, ds, \tag{23}$$

where $g(s) = (1 - e^{-\gamma(t-s)})/m\gamma$.

Reasoning as above, we find that the stochastic integral in equation (23) is a normal variable with zero mean and covariance matrix $\boldsymbol{\Sigma} = \sigma^2 \boldsymbol{I}$, where

$$\sigma^2 = q \int_0^t g^2(s) \, ds = \frac{q}{2\gamma^3}(2\gamma t - 3 + 4e^{-\gamma t} - e^{-2\gamma t}). \tag{24}$$

The moments of the displacement are

$$\mathbb{E}\left[\boldsymbol{x}(t) - \boldsymbol{x}_0 - \boldsymbol{v}_0 \frac{1 - e^{-\gamma t}}{\gamma} \right] = 0 \tag{25}$$

and the conditional second moment of the displacement is

$$\mathbb{E}(|\boldsymbol{x}(t) - \boldsymbol{x}_0|^2 \mid \boldsymbol{x}_0, \boldsymbol{v}_0) = \int |\boldsymbol{x} - \boldsymbol{x}_0|^2 p\,(\boldsymbol{x}, t \mid \boldsymbol{x}_0, \boldsymbol{v}_0) \, d\boldsymbol{x}$$
$$= \frac{|\boldsymbol{v}_0|^2}{\gamma^2}(1 - e^{-\gamma t})^2 + \frac{3kT}{m\gamma^2}(2\gamma t - 3 + 4e^{-\gamma t} - e^{-2\gamma t}), \tag{26}$$

which is independent of $\boldsymbol{x}_0$. Using the Maxwell distribution of velocities (14), we find that the unconditional second moment is

$$\begin{aligned}
\mathbb{E}\,|\boldsymbol{x}(t) - \boldsymbol{x}_0|^2 &= \mathbb{E}_{\boldsymbol{x}_0}\mathbb{E}_{\boldsymbol{v}_0}(|\boldsymbol{x}(t) - \boldsymbol{x}_0|^2 \mid \boldsymbol{x}_0, \boldsymbol{v}_0) \\
&= \frac{3kT}{m\gamma^2}(1 - e^{-\gamma t})^2 + \frac{3kT}{m\gamma^2}(2\gamma t - 3 + 4e^{-\gamma t} - e^{-2\gamma t}) \\
&= \frac{6kT}{m\gamma^2}(\gamma t - 1 + e^{-\gamma t}).
\end{aligned} \tag{27}$$

The long time asymptotics of $\mathbb{E}\,|\boldsymbol{x}(t) - \boldsymbol{x}_0|^2$ is found from (27) to be

$$\mathbb{E}\,|\boldsymbol{x}(t) - \boldsymbol{x}_0|^2 \sim \frac{6kT}{m\gamma}t = \frac{kT}{ma\eta}t \quad \text{for } t\gamma \gg 1; \tag{28}$$

that is, the displacement variance of each component is asymptotically $kT/3ma\eta$. It was this fact that was verified experimentally by Perrin [21]. The one-dimensional diffusion coefficient, as defined in (4), is therefore given by $D = kT/6ma\eta$.

Equation (27) implies that the short time asymptotics of $\mathbb{E}\,|\boldsymbol{x}(t) - \boldsymbol{x}_0|^2$ is given by

$$\mathbb{E}\,|\boldsymbol{x}(t) - \boldsymbol{x}_0|^2 \sim \frac{3kT}{m}t^2 = \langle|\boldsymbol{v}_0|^2\rangle t^2. \tag{29}$$

This result was first obtained by Smoluchowski.

3.4. Reconciliation of Einstein's and Langevin's theories

To reconcile the Einstein and the Langevin approaches, we have to show that for two disjoint time intervals, (t_1, t_2) and (t_3, t_4), in the limit $\gamma \to \infty$, the increments $\Delta_1\boldsymbol{x} = \boldsymbol{x}(t_2) - \boldsymbol{x}(t_1)$ and $\Delta_3\boldsymbol{x} = \boldsymbol{x}(t_4) - \boldsymbol{x}(t_3)$ are independent zero mean Gaussian variables with variances proportional to the time increments. Equation (23) implies that in the limit $\gamma \to \infty$ the increments $\Delta_1\boldsymbol{x}$ and

$\Delta_3 \boldsymbol{x}$ are zero mean Gaussian variables and (28) shows that the variance of an increment is proportional to the time increment.

To show that the increments are independent, we use (20) in (23) to obtain

$$\lim_{\gamma \to \infty} \gamma^2 \langle \Delta_1 \boldsymbol{x} \cdot \Delta_3 \boldsymbol{x} \rangle = \lim_{\gamma \to \infty} \int_{t_1}^{t_2} \int_{t_3}^{t_4} \langle \gamma \boldsymbol{v}(s_1) \cdot \gamma \boldsymbol{v}(s_2) \rangle \, ds_1 \, ds_2$$

$$= \frac{2q}{m^2} \int_{t_1}^{t_2} \int_{t_3}^{t_4} \delta(s_2 - s_1) \, ds_1 \, ds_2 = 0. \tag{30}$$

As is well-known [30], uncorrelated Gaussian variables are independent. This reconciles the Einstein and Langevin theories of Brownian motion in liquid.

Introducing the dimensionless variables $s = \gamma t$ and $\boldsymbol{\xi}(s) = \sqrt{m/6kT}\,\gamma \boldsymbol{x}(t)$, we find from (27) that

$$\lim_{\gamma \to \infty} \mathbb{E}\, |\boldsymbol{\xi}(s) - \boldsymbol{\xi}(0)|^2 = s - 1 + e^{-s} \sim s \text{ for } s \gg 1 \tag{31}$$

and from (30) that

$$\lim_{\gamma \to \infty} \mathbb{E}[\Delta_1 \boldsymbol{\xi} \cdot \Delta_3 \boldsymbol{\xi}] = 0. \tag{32}$$

Equations (31) and (32) explain (in the context of Langevin's description) Einstein's quoted assumption that ' ... *the movement of one and the same particle after different intervals of time (are) mutually independent processes, so long as we think of these intervals of time as being chosen not too small*'.

4. Smoluchowski's limit of Langevin's equation

The Langevin equation (13) serves as a model for many activated processes [31], for which the escape rate determines their time evolution. It is one of the most extensively studied equations in statistical physics [32]. For high damping, the joint probability density function (pdf) of displacement $x(t)$ and velocity $\dot{x}(t)$ breaks into a product of the stationary Maxwellian pdf of the velocity $v = \dot{x}$ and the time-dependent pdf of the displacement $x(t)$, which satisfies an altogether different equation. This is the case not only for the linear Langevin equation, but holds in general.

Smoluchowski has shown [3] that as $\gamma \to \infty$ the trajectories $x(t)$ of the Langevin equation (13) converge in probability to these of the Smoluchowski equation

$$\gamma \dot{x} + U'(x) = \sqrt{2\varepsilon\gamma}\,\dot{w}, \tag{33}$$

where $\dot{w}(t) = \Xi(t)$ is δ-correlated Gaussian white noise.

A more modern derivation begins with writing the Langevin equation (13) as the phase space system

$$\dot{x} = v \tag{34}$$

$$\dot{v} = -\gamma v - U'(x) + \sqrt{2\varepsilon\gamma}\,\dot{w}, \tag{35}$$

and with scaling time by setting

$$t = \gamma s. \tag{36}$$

The scaled Brownian motion $w(t) = \sqrt{\gamma}\,w^{\gamma}(s)$, $w^{\gamma}(s)$ is a standard Brownian motion in time s. The scaled white noise is formally

$$\dot{w}(t) = \gamma^{-1} \mathrm{d} \sqrt{\gamma}\, w^\gamma(s)/\mathrm{d}s = \gamma^{-1/2} \overset{\circ}{w}{}^\gamma(s).$$

Setting $x^\gamma(s) = x(\gamma t)$, $v^\gamma(s) = v(\gamma t)$, and using the overcircle notation for the derivative with respect to s, we note that $\dot{x}(t) = \gamma^{-1} \overset{\circ}{x}{}^\gamma(s)$, $\dot{v}(t) = \gamma^{-1} \overset{\circ}{v}{}^\gamma(s)$, (35) takes the form

$$\overset{\circ}{v}{}^\gamma(s) + \gamma^2 v^\gamma(s) = -\gamma U'(x^\gamma(s)) + \gamma \sqrt{2\varepsilon}\, \overset{\circ}{w}{}^\gamma(s).$$

Hence

$$v^\gamma(s) = v^\gamma(0) \mathrm{e}^{-\gamma^2 s} + \gamma \int_0^s \mathrm{e}^{-\gamma^2(s-u)}[-U'(x^\gamma(u))\,\mathrm{d}u + \sqrt{2\varepsilon}\,\mathrm{d}w^\gamma(u)],$$

which can be written as $\dot{x}(t) = \gamma^{-1} \overset{\circ}{x}{}^\gamma(s) = v^\gamma(s)$, so that

$$x^\gamma(s) = x^\gamma(0) + \gamma \int_0^s v^\gamma(z)\,\mathrm{d}z = x^\gamma(0) + v^\gamma(0) \frac{1 - \mathrm{e}^{-\gamma^2 s}}{\gamma}$$
$$+ \gamma^2 \int_0^s \int_0^z \mathrm{e}^{-\gamma^2(z-u)}[-U'(x^\gamma(u))\,\mathrm{d}u + \sqrt{2\varepsilon}\,\mathrm{d}w^\gamma(u)]\,\mathrm{d}z.$$

In the limit $\gamma \to \infty$

$$x^\infty(s) = x^\infty(0) + \int_0^s [-U'(x^\infty(u))\,\mathrm{d}u + \sqrt{2\varepsilon}\,\mathrm{d}w^\infty(u)],$$

where $w^\infty(u)$ is Brownian motion. This is the integral form of the Smoluchowski stochastic differential equation

$$\overset{\circ}{x}{}^\gamma(s) = -U'(x^\infty(s)) + \sqrt{2\varepsilon}\, \overset{\circ}{w}{}^\infty(s). \tag{37}$$

Returning to the original time scale, (37) becomes (33), which means that (37) is the Langevin equation (13) without the inertia term $\ddot{x}$. This means that the limit exists on every trajectory.

4.1. Numerical solution of the Smoluchowski equation

Starting with the Smoluchowski equation in dimension $d \geqslant 1$

$$\dot{x}(t) = a(x(t), t) + b(x(t), t)\,\dot{w}(t), \tag{38}$$

where x and $a(x, t)$ are d-dimensional vectors, $w(t)$ is an m-dimensional Brownian motion, and $b(x, t)$ is a $d \times m$ matrix, approximate trajectories of (38) can be constructed on any time interval $s < t < T$ by the Euler scheme

$$x(t + \Delta t) = x(t) + a(x(t), t)\Delta t + b(x(t), t)\,\Delta w(t, \Delta t) \tag{39}$$

$$x_N(s) = x_0.$$

Boundary behavior can be imposed on the trajectories of (39) in a given domain D. For example, all trajectories of (39) can be instantaneously terminated when they exit D. In this case the boundary ∂D is called *an absorbing boundary*. The trajectories can be instantaneously reflected at ∂D back into D according to a given reflection law; in this case ∂D is called *a reflecting boundary*. They can also be either instantaneously terminated with a given probability or instantaneously reflected; then ∂D is called *a partially reflecting boundary*.

It can be shown that the trajectories of (39) with a given boundary behavior converge to a limit as $\Delta t \to 0$. The limit is defined as the solution of the Smoluchowski equation (38) with

the given boundary behavior. (see [18] and [55] for details and for other types of boundary behavior.)

4.2. The probability density of the Smoluchowski trajectories

We assume that in the one-dimensional case $b(x, t) > \delta > 0$ for some constant δ. We assume for now that $a(x,t)$ and $b(x,t)$ are deterministic functions. To construct the pdf of a trajectory of (39), we note that the pdf of $x_N(t)$ can be expressed explicitly for t on the lattice, because (39), written as

$$\Delta w(t) = \frac{x_N(t + \Delta t) - x_N(t) - a(x_N(t), t)}{b(x_N(t), t)}, \tag{40}$$

means that for all t on the lattice the expressions on the right-hand side of (40) are independent, identically distributed Gaussian variables. It follows that the pdf of the entire Euler trajectory is the product

$$p(x_1, t_1; x_2, t_2; \ldots; x_n, t_n)$$
$$= \prod_{k=1}^{n} [2\pi b^2(x_{k-1}, t_{k-1})\Delta t]^{-1/2} \exp\left\{ -\frac{[x_k - x_{k-1} - a(x_{k-1}, t_{k-1})\Delta t]^2}{2b^2(x_{k-1}, t_{k-1})\Delta t} \right\}. \tag{41}$$

Setting $x_n = x$ and integrating over $\mathbb{R}$ with respect to all intermediate points $x_1, x_2, \ldots, x_{n-1}$, we find from (41) that the transition pdf of the trajectory satisfies on the lattice the recurrence relation

$$p_N(x, t + \Delta t \mid x_0) = \int_{\mathbb{R}} \frac{p_N(y, t \mid x_0)\, \mathrm{d}y}{\sqrt{2\pi\Delta t}\, b(y, t)} \exp\left\{ -\frac{[x - y - a(y, t)\Delta t]^2}{2b^2(y, t)\Delta t} \right\}. \tag{42}$$

The solution of the integral equation (42) is called Wiener's *discrete path integral*. Its limit as $N \to \infty$ is called Wiener's *path integral*.

For $\Delta t = (t - s)/N$, in the limit $N \to \infty$, the pdf $p_N(x, t \mid x_0)$ of the solution $x_N(t, \mathfrak{w})$ of (39) converges to the solution $p(x, t \mid x_0)$ of (42), where $\mathfrak{w}$ is the entire discrete path of the Brownian motion $w(t)$ on the lattice. Expansion of $p_N(x, t \mid x_0)$ in (42) shows that the pdf $p(x, t \mid x_0)$ is also the solution of the initial value problem

$$\frac{\partial p(y, t \mid x, s)}{\partial t} = \frac{1}{2} \frac{\partial^2 [b^2(y, t)p(y, t \mid x, s)]}{\partial y^2} - \frac{\partial [a(y, t)p(y, t \mid x, s)]}{\partial y} \tag{43}$$

with the initial condition

$$\lim_{t \downarrow s} p(y, t \mid x, s) = \delta(y - x). \tag{44}$$

Equation (43) is called the *Fokker–Planck–(Smoluchowski) equation (FPE)* (see [55]).

In the Smoluchowski equation (38) for $d = n \geqslant 1$, the $n \times m$ matrix

$$\boldsymbol{B}(\boldsymbol{x}, t) = \{b^{ij}(\boldsymbol{x}, t)\}_{n \times m} \tag{45}$$

is called the *noise matrix*, and $\boldsymbol{\sigma}(\boldsymbol{x}, t) = \frac{1}{2}\boldsymbol{B}(\boldsymbol{x}, t)\boldsymbol{B}^T(\boldsymbol{x}, t)$ is called the *diffusion matrix*. The operator

$$\mathcal{L}_y p = \sum_{i=1}^{d} \frac{\partial}{\partial y^i} \left\{ \sum_{j=1}^{d} \frac{\partial}{\partial y^j} \sigma^{ij}(\boldsymbol{y}, t)p - a^i(\boldsymbol{y}, t)p \right\}, \tag{46}$$

is called the *Fokker–Planck operator*, or the *forward Kolmogorov operator.*

As in the one-dimensional case, the pdf $p(\mathbf{y}, t \mid \mathbf{x}, s)$ that $\mathbf{x}(t) = \mathbf{y}$, given that $\mathbf{x}(s) = \mathbf{x}$, is the solution of the Fokker–Planck–Smoluchowski initial value problem

$$\frac{\partial p(\mathbf{y}, t \mid \mathbf{x}, s)}{\partial t} = \mathcal{L}_{\mathbf{y}} p(\mathbf{y}, t \mid \mathbf{x}, s) \text{ for } \mathbf{x}, \mathbf{y} \in \mathbb{R}^n, \ t > s, \tag{47}$$

$$\lim_{t \downarrow s} p(\mathbf{y}, t \mid \mathbf{x}, s) = \delta(\mathbf{x} - \mathbf{y}). \tag{48}$$

It can be written as the conservation law by defining the probability flux density vector

$$J^i(\mathbf{y}, t \mid \mathbf{x}, s) = -\sum_{j=1}^{d} \frac{\partial}{\partial y^j} \sigma^{ij}(\mathbf{y}, t) p(\mathbf{y}, t \mid \mathbf{x}, s) - a^i(\mathbf{y}, t) p(\mathbf{y}, t \mid \mathbf{x}, s) \tag{49}$$

and writing (47) in the divergence form

$$\frac{\partial p(\mathbf{y}, t \mid \mathbf{x}, s)}{\partial t} = -\mathrm{div}_{\mathbf{y}} \mathbf{J}(\mathbf{y}, t \mid \mathbf{x}, s). \tag{50}$$

The probability density at time t and at point $\mathbf{x}$ can be represented for any domain Ω by the limit as $N \to \infty$ of

$$\Pr\{\mathbf{x}_N(t_{1,N}) \in \Omega, \mathbf{x}_N(t_{2,N}) \in \Omega, \ldots, \mathbf{x}_N(t) = \mathbf{x}, t \leqslant T \leqslant t + \Delta t \mid \mathbf{x}(0) = \mathbf{y}\}$$

$$= \left[\int_{\Omega} \int_{\Omega} \cdots \int_{\Omega} \prod_{j=1}^{N} \frac{\mathrm{d}\mathbf{y}_j}{\sqrt{(2\pi\Delta t)^n \det \boldsymbol{\sigma}(\mathbf{x})(t_{j-1,N})}} \right.$$

$$\times \exp\left\{ -\frac{1}{2\Delta t} \left[\mathbf{y}_j - \mathbf{x}(t_{j-1,N}) - \mathbf{a}(\mathbf{x}(t_{j-1,N}))\Delta t\right]^T \boldsymbol{\sigma}^{-1}(\mathbf{x}(t_{j-1,N})) \right.$$

$$\left. \times \left[\mathbf{y}_j - \mathbf{x}(t_{j-1,N}) - \mathbf{a}(\mathbf{x}(t_{j-1,N}))\Delta t\right] \right\}, \tag{51}$$

where

$$\Delta t = \frac{t}{N}, \quad t_{j,N} = j\Delta t,$$

and

$$\mathbf{x}(t_{0,N}) = \mathbf{y}$$

in the product. The limit is the Wiener integral defined by the stochastic differential equation (38) with appropriate boundary condition. In the limit $N \to \infty$ the integral (51) converges to the solution of the Fokker–Planck equation (50) in Ω. Similarly, expanding the path integral with respect to $\mathbf{x}$ and s, we find that $p(\mathbf{y}, t \mid \mathbf{x}, s)$ satisfies the *backward Kolmogorov equation* [18]

$$\mathcal{L}_{\mathbf{x}}^* p(\mathbf{y}, t \mid \mathbf{x}, s) = \sum_{i=1}^{n} \sum_{j=1}^{n} \sigma^{ij}(\mathbf{x}, s) \frac{\partial^2 p(\mathbf{y}, t \mid \mathbf{x}, s)}{\partial x^i \partial x^j} + \sum_{i=1}^{n} a^i(\mathbf{x}, s) \frac{\partial p(\mathbf{y}, t \mid \mathbf{x}, s)}{\partial x^i} \tag{52}$$

with the terminal condition

$$\lim_{t \uparrow s} p(\mathbf{y}, t \mid \mathbf{x}, s) = \delta(\mathbf{y} - \mathbf{x}). \tag{53}$$

The Fokker–Planck equation can be generalized when a killing measure is added to the dynamics. A killing measure represents the probability per unit time and unit length to terminate a trajectory at a given point at a given time. Mixed boundary conditions and Fokker–Planck equation for the survival probability with killing is discussed in [14].

4.3. Diffusion processes and diffusion models of large data sets

A d-dimensional Markov process $\boldsymbol{x}(t)$ is called a *diffusion process* with (deterministic) drift vector field $\boldsymbol{a}(\boldsymbol{x}, t)$ and *(deterministic) diffusion matrix* $\boldsymbol{\sigma}(\boldsymbol{x}, t)$, if it has continuous trajectories,

$$\lim_{\Delta t \to 0} \frac{1}{\Delta t} \mathbb{E}\{\boldsymbol{x}(t + \Delta t) - \boldsymbol{x}(t) \,|\, \boldsymbol{x}(t) = \boldsymbol{x}\} = \boldsymbol{a}(\boldsymbol{x}, t) \tag{54}$$

$$\lim_{\Delta t \to 0} \frac{1}{\Delta t} \mathbb{E}\left\{ [x^i(t + \Delta t) - x^i(t)][x^j(t + \Delta t) - x^j(t)] \,|\, \boldsymbol{x}(t) = \boldsymbol{x} \right\} = \sigma^{ij}(\boldsymbol{x}, t) \tag{55}$$

for $i, j = 1, 2, \ldots, d$, and for some $\delta > 0$

$$\lim_{\Delta t \to 0} \frac{1}{\Delta t} \mathbb{E}\{ |\boldsymbol{x}(t + \Delta t) - \boldsymbol{x}(t)|^{2+\delta} \,|\, \boldsymbol{x}(t) = \boldsymbol{x} \} = 0.$$

It can be shown [18] that under mild regularity assumptions on the coefficient the solution of the stochastic differential equation (SDE)

$$\dot{\boldsymbol{x}}(t) = \boldsymbol{a}(\boldsymbol{x}(t), t) + \boldsymbol{B}(\boldsymbol{x}(t), t)\, \dot{\boldsymbol{w}}(t) \tag{56}$$

is a diffusion process with drift field $\boldsymbol{a}(\boldsymbol{x}, t)$ and diffusion matrix $\boldsymbol{\sigma}(\boldsymbol{x}, t) = \frac{1}{2}\boldsymbol{B}(\boldsymbol{x}, t)\boldsymbol{B}^T(\boldsymbol{x}, t)$. Also a partial converse is true: given sufficiently nice drift field $\boldsymbol{a}(\boldsymbol{x}, t)$ and a strictly positive definite diffusion matrix $\boldsymbol{\sigma}(\boldsymbol{x}, t)$ of a diffusion process, there is a noise matrix $\boldsymbol{B}(\boldsymbol{x}, t)$ and a Brownian motion $\boldsymbol{w}(t)$ such the process is a solution of the SDE (56) [18, 19].

Equations (54) and (55) reconstruct the SDE from its trajectories. The discrete version of these equations can be used as approximations to the coefficients, when a sufficiently large set of trajectory fragments is given (see [56, 58, 59]). Indeed, large number (tens of thousands) of short single particle trajectories (SPTs), collected by super-resolution methods, at tens of nanometer precision for motion occurring in cell are ideal data to recover drift and diffusion tensors. But the sampled molecular process cannot be directly modeled by the overdamped Langevin equation, which describes diffusion on the microscopic level, because an additional noise of localization is added in tracking the motion (algorithm and point spread function error). Using a stochastic model of the acquired data to calibrate the model, it is possible to distinguish the perturbation added to the physical motion (stochastic equation) [58]. The denoising procedure of the SPTs reveals that effective diffusion coefficient contains the divergence of deterministic drift component and also provides a criteria to differentiate trapped stochatic particle from immobile ones [58].

4.4. The MFPT and survival probability

If the Smoluchowski trajectories are terminated at the boundary ∂D of a given domain, the pdf vanishes on ∂D. Thus equations (47) and (48) have to be supplemented by the boundary condition

$$p(\boldsymbol{y}, t \,|\, \boldsymbol{x}, s) = 0 \text{ for } \boldsymbol{y} \in \partial D, \ \boldsymbol{x} \in D, \ t > s. \tag{57}$$

In this case, the first passage time to the boundary ∂D is

$$\tau_D = \inf\{t : \boldsymbol{x}(t) \notin D\}. \tag{58}$$

Thus, the probability that the Smoluchowski trajectory is still in D at time $t > s$, given that at time $s < t$ it started at $\boldsymbol{x} \in D$, is given by

$$\Pr\{\boldsymbol{x}(t) \in D \mid \boldsymbol{x}(s) = \boldsymbol{x}\} = \int_D p(\boldsymbol{y}, t \mid \boldsymbol{x}, s) \, \mathrm{d}\boldsymbol{y} \tag{59}$$

Actually, $\Pr\{\boldsymbol{x}(t) \in D \mid \boldsymbol{x}(s) = \boldsymbol{x}\} = \Pr\{\tau_D > t \mid \boldsymbol{x}(s) = \boldsymbol{x}\}$, which is *the survival probability* at time $t > s$ of the Smoluchowski trajectory that started at $\boldsymbol{x}$ at time $s < t$.

If the Smoluchowski trajectories are reflected at the boundary ∂D of a given domain such that the normal flux at the boundary vanishes [16], then the boundary condition becomes

$$\boldsymbol{J}(\boldsymbol{y}, t \mid \boldsymbol{x}, s) \cdot \boldsymbol{\nu}(\boldsymbol{y}) = 0 \text{ for } \boldsymbol{y} \in \partial D, \boldsymbol{x} \in D, \ t > s, \tag{60}$$

where $\boldsymbol{\nu}(\boldsymbol{y})$ is the unit outer normal vector at $\boldsymbol{y} \in \partial D$.

When the boundary ∂D absorbs the Smoluchowski trajectories, the expected MFPT to the boundary of Smoluchowski trajectories in D is found by integrating the survival probability to obtain the MFPT as

$$\mathbb{E}[\tau_D \mid \boldsymbol{x}(s) = \boldsymbol{x}] = \int_s^\infty \int_D p(\boldsymbol{y}, t \mid \boldsymbol{x}, s) \, \mathrm{d}\boldsymbol{y} \, \mathrm{d}t. \tag{61}$$

Setting $u(\boldsymbol{x}, s) = \mathbb{E}[\tau_D \mid \boldsymbol{x}(s) = \boldsymbol{x}]$, using the backward Kolmogorov equation and Green's identity, we obtain the backward boundary value problem

$$\mathcal{L}^*_{\boldsymbol{x}} u(\boldsymbol{x}, s) + \frac{\partial u(\boldsymbol{x}, s)}{\partial s} = -1 \text{ for } \boldsymbol{x} \in D, \tag{62}$$

$$u(\boldsymbol{x}, s) = 0 \text{ for } \boldsymbol{x} \in \partial D. \tag{63}$$

Note that if the coefficients $\boldsymbol{\sigma}$ and $\boldsymbol{a}$ are time-independent, then (52), (63) reduce to the time-homogeneous elliptic Pontryagin–Andronov–Vitt (PAV) [17] boundary value problem in D

$$\mathcal{L}^*_{\boldsymbol{x}} u(\boldsymbol{x}) = -1 \text{ for } \boldsymbol{x} \in D, \tag{64}$$

$$u(\boldsymbol{x}) = 0 \text{ for } \boldsymbol{x} \in \partial D. \tag{65}$$

If the boundary is reflecting, then the absorbing boundary condition (65) for the PAV equation (64) is changed to

$$\boldsymbol{J}(\boldsymbol{x}) \cdot \boldsymbol{\nu}(\boldsymbol{x}) = 0 \text{ for } \boldsymbol{x} \in \partial D. \tag{66}$$

If ∂D is absorbing on a part ∂D_a and reflecting on the remaining part $\partial D_r - \partial D - \partial D_a$, then the boundary conditions for the PAV equation is absorbing on ∂D_a and reflecting on ∂D_b.

Note further that the MFPT to the boundary is given by (61) , where $p(\boldsymbol{y}, t \mid \boldsymbol{x}, s)$ is the solution of the FPE with absorbing boundary conditions also in the case of reflecting boundaries, because prior to reaching the boundary the Smoluchowski trajectories are independent of boundary behavior.

5. Modeling in cell using the stochastic narrow escape

The narrow escape problem is to evaluate the MFPT when the reflecting part of the boundary ∂D_b is much bigger than the absorbing part ∂D_a [35, 36, 38, 39, 40–42, 44, 45]. In this case ∂D_a
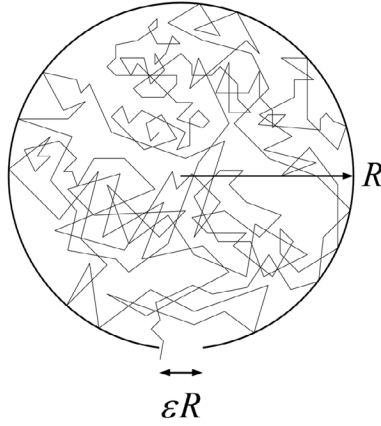
Figure 1. Brownian trajectory escaping through a small absorbing window a domain with otherwise reflecting boundary .

represents a small absorbing window in the boundary, through which trajectories can escape the domain D, while the large reflecting part ∂D_b represents an impermeable wall (figure 1), such as a lipid cell membrane that is impermeable to diffusing ions. This mathematical model represents many biological models. Thus equation (64) and the boundary conditions (65) or (66) are the basis for the analysis of the narrow escape problem. The MFPT $\bar{\tau}$ depends on the starting point x of the Brownian trajectory, thus it should be denoted $\bar{\tau}(x)$. This function is the solution of the classical mixed Neumann-Dirichlet boundary value problem for the Laplace equation [14, 18],

$$D\nabla^2\bar{\tau}(x) = -1 \text{ for } x \in \Omega \tag{67}$$

$$\frac{\partial\bar{\tau}(x)}{\partial n} = 0 \text{ for } x \in \partial\Omega_r \tag{68}$$

$$\bar{\tau}(x) = 0 \text{ for } x \in \partial\Omega_a\,, \tag{69}$$

where D is the diffusion coefficient and n is the unit outer normal to the boundary [18]. The system (67)–(69) follows from the backward Kolmogorov equation [18] (the adjoint of the Fokker–Planck equation) for the transition probability density function $p(y, t\,|\,x)$ of the Brownian trajectories,

$$\frac{\partial p(y, t\,|\,x)}{\partial t} = D\nabla_x^2 p(\,y, t\,|\,x) \text{ for } x, y \in \Omega \tag{70}$$

$$\frac{\partial p(y, t\,|\,x)}{\partial n_x} = 0 \text{ for } y \in \Omega, x \in \Omega_r \tag{71}$$

$$p(y, t\,|\,x) = 0 \text{ for } y \in \Omega, x \in \Omega_a \tag{72}$$

$$p(y, 0\,|\,x) = \delta(\,y - x) \text{ for } x, y \in \Omega\,. \tag{73}$$

The survival probability of Brownian trajectories that start at $\boldsymbol{x} \in \Omega$ is

$$\Pr\{\tau > t \mid \boldsymbol{x}\} = \int_{\Omega} p(\boldsymbol{y}, t \mid \boldsymbol{x}) \, \mathrm{d}\boldsymbol{y} \tag{74}$$

and its mean value is

$$\bar{\tau}(\boldsymbol{x}) = \int_0^{\infty} \Pr\{\tau > t \mid \boldsymbol{x}\} \, \mathrm{d}t. \tag{75}$$

It follows that

$$D\nabla^2 \bar{\tau}(\boldsymbol{x}) = \int_0^{\infty} D\nabla_{\boldsymbol{x}}^2 \Pr\{\tau > t \mid, \boldsymbol{x}\} \, \mathrm{d}t = \int_0^{\infty} \int_{\Omega} \frac{\partial p(\boldsymbol{y}, t \mid \boldsymbol{x})}{\partial t} \, \mathrm{d}\boldsymbol{y} \, \mathrm{d}t = -1. \tag{76}$$

The last equality in (76) follows from the initial condition (73) and the Neumann and Dirichlet conditions (68) and (69) are inherited from (71) and (72), respectively.

No explicit solutions to the problem (67)–(69) are known in general [14]. If the absorbing part of the boundary $\partial \Omega_a$ is much smaller than the entire boundary $\partial \Omega$, numerical solutions to the problem are very hard to construct due to the presence of a boundary layer near $\partial \Omega_a$, where gradients are very large so the numerical complexity becomes prohibitive. The problem cannot be circumvented by Brownian dynamics simulations of the MFPT $\bar{\tau}$, because reaching $\partial \Omega_a$ is a rare event on the time scale of diffusion. The remedy to these difficulties is the construction of analytical approximations to the solution of (67)–(69) by new asymptotic methods developed specifically for the problem at hand. In the next section, we summarize the asymptotic formulas solution of (67)–(69). We briefly mention how they are derived and refer to [14] for more details.

5.1. Narrow escape formula in two-dimensions

We summarize here the asymptotic formulas of the MFPT (67) when the domain Ω is in the plane and absorbing boundary is a small sub arc $\partial \Omega_a$ (of length a) of the boundary $\partial \Omega$. We have reviewed the mathematical method and the analysis in [60, 62]. There is little intuition behind these formulas and it is not fruitful to guess what there are. It is indeed hard to tell in advance how the geometry enters into the formulas. The recipe we adopted is to follow the analytical derivations that reveal how local and global structures, smoothness or not, local curvature controls the narrow escape time.

1. When $\partial \Omega_a$ is a sub-arc of a smooth boundary, the MFPT from any point $\boldsymbol{x}$ in Ω to $\partial \Omega_a$ is denoted $\bar{\tau}_{\boldsymbol{x} \to \partial \Omega_a}$. For

$$\varepsilon = \frac{\pi |\partial \Omega_a|}{|\partial \Omega|} = \frac{\pi a}{|\partial \Omega|} \ll 1 \tag{77}$$

the MFPT is independent of $\boldsymbol{x}$ outside a small vicinity of $\partial \Omega_a$ (called a boundary layer). Thus for $\boldsymbol{x} \in \Omega$, outside a boundary layer near $\partial \Omega_a$,

$$\bar{\tau}_{\boldsymbol{x} \to \partial \Omega_a} = \frac{|\Omega|}{\pi D} \ln \frac{1}{\varepsilon} + O(1), \tag{78}$$

where $O(1)$ depends on the initial distribution of $\boldsymbol{x}$ [35–57]. This result was derived independently using matched asymptotic technics and Green's function method.
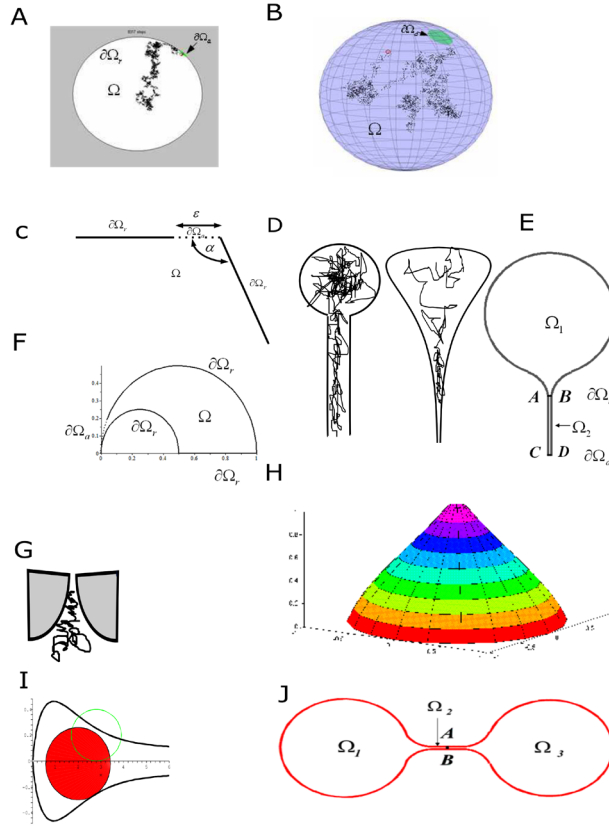
Figure 2. Classification of NET formula. (A) The absorbing boundary $\partial\Omega_a$ is a short arc (marked green) of the smooth boundary curve $\partial\Omega$. (B) $\partial\Omega_a$ is an absorbing disk arc (marked green) on a surface. (C) $\partial\Omega_a$ is a short arc at a corner arc (marked ε). (D) $\partial\Omega_a$ is an absorbing segment (resp. circle) at the end of a narrow strip (resp. cylinder) connected non-smoothly to the head in a planar (resp. surface of revolution) dendritic spine model. (E) $\partial\Omega_a$ is a short segment CD at the end of the narrow strip Ω_2 in the plane or a circle at the end of the narrow cylinder Ω_2 on a surfaced of revolution connected smoothly to the head. (F) $\partial\Omega_a$ is a short arc at a boundary cusp arc (marked ε). (G) $\partial\Omega_a$ is a narrow opening at the end of a cusp-like funnel. (H) $\partial\Omega_a$ is an opening at the end of a funnel of finite angle . (I) The narrow passage is formed by an obstacle. (J) A dumbbell-shaped domain.

If Ω is a disc of radius R, then for $\boldsymbol{x}$ at the center of the disk (figure 2(A)),

$$\bar{\tau}_{\boldsymbol{x}\to\partial\Omega_a} = \frac{R^2}{D}\left[\log\frac{R}{a} + 2\log 2 + \frac{1}{4} + O(\varepsilon)\right],$$

and averaging with respect to a uniform distribution of $\boldsymbol{x}$ in the disk [14]

$$\bar{\tau} = \frac{R^2}{D}\left[\log\frac{R}{a} + 2\log 2 + \frac{1}{8} + O(\varepsilon)\right].$$

This result was obtained from generalizing Sneddon's method for mixed boundary value problem. The method is based on Abel's transformation [40–42]. The flux through a hole in a smooth wall on a flat membrane surface is regulated by the area $|\Omega|$ inside the wall, the diffusion coefficient D, and the aspect ratio ε (77). In the case of Brownian motion on a sphere of radius R the MFPT to an absorbing circle centered on the north-south axis near the south pole with small radius $a = R \sin \delta/2$ is given by

$$\bar{\tau} = \frac{2R^2}{D} \log \frac{\sin \frac{\theta}{2}}{\sin \frac{\delta}{2}}, \tag{79}$$

where θ is the angle between $\boldsymbol{x}$ and the south-north axis of the sphere (figure 2(B)).

2. If the absorbing window is located at a corner of angle α, then

$$\bar{\tau} = \frac{|\Omega|_g}{D\alpha} \left[\log \frac{1}{\varepsilon} + O(1) \right], \tag{80}$$

where $|\Omega|_g$ is the surface area of the domain on the curved surface, calculated according to the Riemannian metric on the surface [40]. Formula (80) indicates that control of flux is regulated also by the access to the absorbing window afforded by the angle of the corner leading to the window (figure 2(C)). This formula was obtained using a conformal map sending a corner to a flat line.

3. If the absorbing window is located at a cusp, then $\bar{\tau}$ grows algebraically, rather than logarithmically. Thus, in the domain bounded between two tangent circles, the expected lifetime is

$$\bar{\tau} = \frac{|\Omega|}{(d^{-1} - 1)D} \left(\frac{1}{\varepsilon} + O(1) \right), \tag{81}$$

where $d < 1$ is the ratio of the radii [42] (figure 2(F)). Formula (81) indicates that a drastic reduction of flux can be achieved by putting an obstacle that limits the access to the absorbing window by forming a cusp-like passage. This formula was derived using the exponential conformal map.

4. When $\partial \Omega_a$ (of length a) is located at the end of a narrow neck with radius of curvature R_c, the MFPT is given in [14, 63] as (figures 2(G) and (I))

$$\bar{\tau} = \frac{|\Omega|}{4D\sqrt{2a/R_c}}(1 + O(1)) \text{ for } a \ll |\partial \Omega|. \tag{82}$$

This formula is derived by a new method that uses a Mobius transformation to resolve the cusp singularity [14, 63]. The boundary layer at the cusp is sent to a banana shaped domain. Asymptotic formula for a general cusp with an arbitrary power law are not known. For a surface of revolution generated by rotating the curve about its axis of symmetry [63], we use the representation of the generating curve

$$y = r(x), \ \Lambda < x < 0$$

where the x-axis is horizontal with $x = \Lambda$ at the absorbing end $\boldsymbol{AB}$. We assume that the parts of the curve that generate the funnel have the form

$$r(x) = O(\sqrt{|x|}) \text{ near } x = 0$$

$$r(x) = a + \frac{(x - \Lambda)^{1+\nu}}{\nu(1+\nu)\ell^\nu}(1 + o(1)) \text{ for } \nu > 0 \text{ near } x = \Lambda, \tag{83}$$

where $a = \frac{1}{2}\overline{AB} = \varepsilon/2$ is the radius of the gap, and the constant ℓ has dimension of length. For $\nu = 1$ the parameter ℓ is the radius of curvature R_c at $x = \Lambda$. The MFPT from the head to the absorbing end AB is given by

$$\bar{\tau} \sim \frac{\mathcal{S}(\Lambda)}{2D} \frac{\left(\frac{\ell}{(1+\nu)a}\right)^{\nu/1+\nu} \nu^{1/1+\nu}}{\sin\frac{\nu\pi}{1+\nu}}, \tag{84}$$

where $\mathcal{S}$ is the entire unscaled area of the surface. In particular, for $\nu = 1$ the MFPT (84) reduces to

$$\bar{\tau} \sim \frac{\mathcal{S}}{4D\sqrt{a/2\ell}}. \tag{85}$$

5. When a bulky head is connected to an essentially one-dimensional strip (or cylinder) of small radius a and length L, as is the case of a neuronal spine membrane (figure 2(D)). The connection of the head to the neck can be at an angle or by a smooth funnel. The boundary of the domain reflects Brownian trajectories and only the end of the cylinder $\partial\Omega_a$ absorbs them. The domain Ω_1 is connected to the cylinder at an interface $\partial\Omega_i$, which in this case is an interval AB. The MFPT from $x \in \Omega_1$ to $\partial\Omega_a$ is given by

$$\bar{\tau}_{x \to \partial\Omega_a} = \bar{\tau}_{x \to \partial\Omega_i} + \frac{L^2}{2D} + \frac{|\Omega_1|L}{|\partial\Omega_a|D}. \tag{86}$$

The flux dependence on the neck length is quite strong. This formula is derived using the additive property of the MFPT [66].

6. A dumbbell-shaped domain (of type (VI)) consists of two compartments Ω_1 and Ω_3 and a connecting neck Ω_2 that is effectively one-dimensional (figure 2(J)), or in a similar domain with a long neck. A Brownian trajectory that hits the segment AB in the center of the neck Ω_2 is equally likely to reach either compartment before the other; thus AB is the stochastic separatrix (SS). Therefore the mean time to traverse the neck from compartment Ω_1 to compartment Ω_3 is asymptotically twice the MFPT $\bar{\tau}_{\Omega_1 \to SS}$. Neglecting, as we may, the mean residence time of a Brownian trajectory in Ω_2 relative to that in Ω_1 or in Ω_3 we can write the transition rates from Ω_1 to the Ω_3 and vv as

$$\lambda_{\Omega_1 \to \Omega_3} = \frac{1}{2\bar{\tau}_{\Omega_1 \to SS}}, \quad \lambda_{\Omega_3 \to \Omega_1} = \frac{1}{2\bar{\tau}_{\Omega_3 \to SS}}. \tag{87}$$

These rates can be found from explicit expressions for the flux into an absorbing window

$$\lambda_1 \sim \frac{1}{\bar{\tau}}, \tag{88}$$

where $\bar{\tau}$ is given in (86). Here $\bar{\tau}_{x \to \partial\Omega_i}$ is any one of the MFPTs given above, depending on the geometry of Ω_1 with L half the length of the neck and with $SS = \partial\Omega_a$. The radii of curvature $R_{c,1}$ and $R_{c,3}$ at the two funnels may be different in Ω_1 and Ω_3. The smallest positive eigenvalue λ of the Neumann problem for the Laplace equation in the dumbbell is to leading order $\lambda = -(\lambda_{\Omega_1 \to \Omega_3} + \lambda_{\Omega_3 \to \Omega_1})$. For example, if the solid dumbbell consists

of two general heads connected smoothly to the neck by funnels (see (93)), the two rates are given by

$$\frac{1}{\lambda_{\Omega_1 \to \Omega_3}} = \sqrt{2} \left[\left(\frac{R_{c,1}}{a} \right)^{3/2} \frac{|\Omega_1|}{R_{c,1}D} \right] (1 + o(1)) + \frac{L^2}{4D} + \frac{|\Omega_1|L}{\pi a^2 D}$$

$$\frac{1}{\lambda_{\Omega_3 \to \Omega_1}} = \sqrt{2} \left[\left(\frac{R_{c,3}}{a} \right)^{3/2} \frac{|\Omega_3|}{R_{c,3}D} \right] (1 + o(1)) + \frac{L^2}{4D} + \frac{|\Omega_3|L}{\pi a^2 D} \tag{89}$$

(see [66]). Formulas (89) indicate that the unidirectional fluxes between the two compartments of a dumbbell-shaped domain can be controlled by the area (or surface area) of the two and by the type of obstacles to the access to the connecting neck. The equilibration rate in the dumbbell, λ, is thus controlled by the geometry.

7. The mean time to escape through N well-separated absorbing windows of lengths a_j at the ends of funnels with radii of curvature ℓ_j, respectively, in the boundary $\partial\Omega$ of a planar domain Ω is given by

$$\bar{\tau} = \frac{\pi|\Omega|}{2D\sum_{j=1}^{N}\sqrt{a_j/\ell_j}}(1 + o(1)) \text{ for } a_j/\ell_j \ll |\partial\Omega|. \tag{90}$$

The probability to escape through window i is given by

$$p_i = \frac{\sqrt{a_i/\ell_i}}{\sum_{j=1}^{N}\sqrt{a_j/\ell_j}}. \tag{91}$$

Formulas (90) and (91) are significant for diffusion in a network of compartments connected by narrow passages (e.g. on a membrane strewn with obstacles). The dependence of the MFPT $\bar{\tau}$ and of the transition probabilities p_i on the local geometrical properties of the compartments renders the effective diffusion tensor in the network position-dependent and can give rise to anisotropic diffusion.

5.2. Narrow escape formula in three-dimension

We now summarize the Narrow Escape Time formula in three-dimensions. The methods are the same as in two dimensions: Matched asymptotic or Greens function and conformal mapping to resolve cusp singularities. Indeed, the axial symmetry allows reducing the three- to two- dimensions and thus to use of conformal transformations [14].

1. The MFPT to a circular absorbing window $\partial\Omega_a$ of small radius a centered at **0** on the boundary $\partial\Omega$ is given by [43]

$$\bar{\tau}_{\boldsymbol{x} \to \partial\Omega_a} = \frac{|\Omega|}{4aD\left[1 + \frac{L(\mathbf{0}) + N(\mathbf{0})}{2\pi}a\log a + o(a\log a)\right]}, \tag{92}$$

where $L(\mathbf{0})$ and $N(\mathbf{0})$ are the principal curvatures of the boundary at the center of $\partial\Omega_a$. This formula was derived using the second order expansion of the Neuman-Green's function at the pole [43].

2. The MFPT from the head of the solid of revolution, obtained by rotating the symmetric domain about its axis of symmetry, to a small absorbing window $\partial\Omega_a$ at the end of a funnel (figure 2(H)) is given by

$$\bar{\tau} = \frac{1}{\sqrt{2}}\left(\frac{R_c}{a}\right)^{3/2}\frac{|\Omega|}{R_c D}(1 + o(1)) \text{ for } a \ll R_c, \tag{93}$$

where the R_c is the radius of curvature of the rotated curve at the end of the funnel [66].

3. The MFPT from a point $\boldsymbol{x}$ in a bulky head Ω to an absorbing disk $\partial\Omega_a$ of a small radius a at the end of a narrow neck of length L, connected to the head at an interface $\partial\Omega_i$ is given by the connection formula (86). When the cylindrical neck is attached to the head at a right angle the interface $\partial\Omega_i$ is a circular disk and $\bar{\tau}_{\boldsymbol{x}\to\partial\Omega_i}$ is given by (92). When the neck is attached smoothly through a funnel, $\bar{\tau}_{\boldsymbol{x}\to\partial\Omega_i}$ is given by (93).

4. The mean time to escape through N well-separated absorbing circular windows or radii a_j at the ends of funnels with curvatures ℓ_j, respectively, is given by

$$\bar{\tau} = \frac{1}{\sqrt{2}}\frac{|\Omega|}{D\sum_{j=1}^{N}\ell_j\left(\frac{a_j}{\ell_j}\right)^{3/2}}. \tag{94}$$

The exit probability through window i is given by

$$p_i = \frac{a_i^{3/2}\ell_i^{-1/2}}{\sum_{j=1}^{N}a_j^{3/2}\ell_j^{-1/2}}. \tag{95}$$

5. The principal eigenvalue of the Laplace equation in a dumbbell-shaped structure is given in item (vi), equations (87)–(89) above [66].

6. The leakage flux through a circular hole of small radius a centered at $\boldsymbol{0}$ in the reflecting boundary is given by [43]

$$J_a = 4aDu_0(\boldsymbol{0}) + O\left(\frac{a^2}{|\Omega|^{2/3}}\log\frac{a}{|\Omega|^{1/3}}\right), \tag{96}$$

where $u_0(\boldsymbol{0})$ is the concentration of diffusers at the window in the same model without the absorbing window.

We refer the reader to the classical literature about the asymptotic formula for narrow escape time [61], the dire Strait time (when escape occurs at a cusp boundary) [63] and the recent monograph [14] for applications in cellular biology.

6. Stochastic Smoluchowski equation for modeling polymer dynamics

A significant application of the Smoluchowski's limit equation is to polymer models. The Rouse model is defined as a collection of beads connected by springs [64]. Monomers are positioned at $\boldsymbol{R}_n$ ($n = 1,2,...N$), subject to Brownian motions and the spring forces are due to the coupling between the nearest neighboring beads. The potential energy is defined by

$$\phi(\boldsymbol{R}) = \frac{\kappa}{2}\sum_{n=1}^{N}(\boldsymbol{R}_n - \boldsymbol{R}_{n-1})^2, \tag{97}$$

In the Rouse model, only neighboring monomers interact [64]. In the Smoluchowski's limit of the Langevin equation, the dynamics of monomer $\boldsymbol{R}_n$ is driven by the potential $\phi(\boldsymbol{R}_1, .., \boldsymbol{R}_N)$, which generates the force $-\nabla_{\boldsymbol{R}_n}\phi(\boldsymbol{R}_1, .., \boldsymbol{R}_N)$. The ensemble of stochastic equations is

$$\frac{\mathrm{d}\boldsymbol{R}_n}{\mathrm{d}t} = -D\kappa(2\boldsymbol{R}_n - \boldsymbol{R}_{n-1} - \boldsymbol{R}_{n+1}) + \sqrt{2D}\frac{\mathrm{d}\boldsymbol{w}_n}{\mathrm{d}t} \tag{98}$$

for $n = 1, ..N$. In this model, at equilibrium all beads are centered at zero, but the variance of the distances in a polymer realization is given by

$$\langle |R_{n+1} - R_n|^2 \rangle = b^2, \tag{99}$$

where b is the standard deviation of the bond length, $\kappa = dk_{\mathrm{B}}T/b^2$ is the spring constant with d the spatial dimension, k_{B} is the Boltzmann coefficient and T the temperature. For a freely-joint-chain polymer, the energy between monomer is changed to

$$\phi(\boldsymbol{R}_1, .., \boldsymbol{R}_N) = \frac{\kappa}{2}\sum_{n=1}^{N}(|\boldsymbol{R}_n - \boldsymbol{R}_{n-1}| - l_0)^2, \tag{100}$$

leading to a steady state configuration, where the mean distance between neighboring beads is $\langle |R_{n+1} - R_n| \rangle = l_0$, where by taking the limit $l_0 = 0$, we recover the classical Rouse model. Starting with a given configuration, the relaxation of a Rouse polymer to steady state in a free space can be analyzed using the Fourier space

$$\boldsymbol{u}_p = \sum_{n=1}^{N}\boldsymbol{R}_n\alpha_p^n, \tag{101}$$

where the change of coordinates is encoded in the matrix

$$\alpha_p^n = \begin{cases} \sqrt{\dfrac{1}{N}}, & p = 0 \\ \sqrt{\dfrac{2}{N}}\cos\left((n - 1/2)\dfrac{p\pi}{N}\right), & \text{otherwise.} \end{cases} \tag{102}$$

$\boldsymbol{u}_0$ represents the motion of the center of mass and the potential ϕ defined in equation (97) is now

$$\phi(\boldsymbol{u}_1, .., \boldsymbol{u}_{N-1}) = \frac{1}{2}\sum_{p=1}^{N-1}\kappa_p\boldsymbol{u}_p^2, \tag{103}$$

where

$$\kappa_p = 4\kappa\sin(\frac{p\pi}{2N})^2. \tag{104}$$

Equations (98) are now decoupled in a $(N-1)d$-independent Ornstein–Uhlenbeck (OU) processes

$$\frac{\mathrm{d}\boldsymbol{u}_p}{\mathrm{d}t} = -D_p\kappa_p\boldsymbol{u}_p + \sqrt{2D_p}\frac{\mathrm{d}\widetilde{\boldsymbol{w}_p}}{\mathrm{d}t}, \tag{105}$$

where $\widetilde{\boldsymbol{w}_p}$ are independent d-dimensional Brownian motions with mean zero and variance 1 and $D_p = D$ for $p = 1..N - 1$, while $D_0 = D/N$ and the relaxation times are defined by

$\tau_p = 1/D\kappa_p$. The center of mass behaves as a freely diffusing particle. Starting from a straight line, the time to relax for a Rouse polymer is dominated by the slowest time constant

$$\tau_N = \frac{1}{D\kappa_1} = \frac{1}{4D\kappa \sin(\frac{1\pi}{2N})^2} \approx \frac{N^2}{D\kappa\pi^2}. \tag{106}$$

6.1. Anomalous motion of a Rouse polymer

The motion of monomer $\boldsymbol{R}_c$ of a Rouse polymer is related to the Fourier coefficients by

$$\boldsymbol{R}_c = \sum_{p=0}^{N-1} \alpha_p^c \boldsymbol{u}_p, \tag{107}$$

where α_p^c are described by relation (102) and $\boldsymbol{u}_p$ satisfy equations (105), which form an ensemble of Ornstein–Uhlenbeck processes, for which the variance is simply

$$\sigma_p^2(t) = \langle |\boldsymbol{u}_p(t) - \boldsymbol{u}_p(0)|^2 \rangle = \frac{1}{\kappa_p}(1 - e^{-2t/\tau_p}), \text{ for } p \geq 1,$$
$$\sigma_0^2(t) = 2D_{\text{cm}}t. \tag{108}$$

The relaxation times are defined by

$$\tau_p = \frac{1}{D\kappa_p}, \tag{109}$$

while the diffusion constant is $D_{\text{cm}} = D/N$. The shortest timescale is $\tau_{N-1} \approx 1/(4D\kappa)$ which is half of the time $\tau_s = 1/(2D\kappa)$ for a free monomer to diffuse a mean squared distance between adjacent monomers ($b^2 = 1/\kappa$). The center of mass is characterized by the time scale $\tau_0 \equiv b^2 N/D_{\text{cm}} = N^2/(D\kappa)$ which is the time for a particle to diffusion across the polymer size. For long polymers $\tau_0/\tau_1 \approx \pi^2$. Using relation (108), the MSD of monomer $\boldsymbol{R}_c$ is a sum of independent OU-variables,

$$\text{var}(\boldsymbol{R}_c(t)) = \langle (\boldsymbol{R}_c(t) - \boldsymbol{R}_c(0))^2 \rangle = \frac{d}{\kappa N} \sum_{p=1}^{N-1} \frac{\cos^2\left(\frac{(2c-1)p\pi}{2N}\right)}{\sin^2(\frac{p\pi}{2N})}(1 - e^{-2t/\tau_p}) + 2dD_{\text{cm}}t, \tag{110}$$

where d is the spatial dimension. Formula (110) shows the deviation with MSD of a Brownian motion, for which the correlation function increases linearly with time. There are three distinguish regimes:

1. For short time $t \ll \tau_{N-1}$, $\sigma_p^2(t) \approx Dt$, independent of p, the sum in equation (110) leads to

   $$\text{var}(\boldsymbol{R}_c) \approx 2dDt, \tag{111}$$

   which is the diffusion regime.
2. For large time, $t \gg \tau_1$, the exponential terms in relation (110) becomes independent of t. Only the first term in equation (108) corresponding to the diffusion of the center of mass gives the time-dependent behavior. This regime is dominated by normal diffusion, with a diffusion coefficient D/N.
3. For intermediate times $\tau_{N-1} \ll t \ll \tau_1$, such that $2t/\tau_p > 1$, the sum of exponentials contributes to equation (110). The variance (110) is

$$\text{var}(R_c) \approx 2 \int_{p_{\min}}^{N-1} \frac{\cos^2\left(\frac{(2c-1)p\pi}{2N}\right)}{\sin^2(\frac{p\pi}{2N})} \mathrm{d}p, \tag{112}$$

where $p_{\min}$ is such that $\tau_{p_{\min}} = 2t$. We have $\text{var}(\boldsymbol{R}_c) \sim t^{1/2}$. A Rouse monomer exhibits anomalous diffusion. The time interval can be arbitrarily long with the size N of the polymer.

6.2. Looping time: a brief summary of an analytical approach

The first looping time between two monomers is the First Encounter Time τ_e for two monomers n_a, n_b to come into a distance $\varepsilon < b$, defined by

$$\tau_e = \inf\{t > 0 \text{ such that } |\boldsymbol{R}_{n_a}(t) - \boldsymbol{R}_{n_b}(t)| \leqslant \varepsilon\}, \tag{113}$$

where $\boldsymbol{R}_{n_a}$ and $\boldsymbol{R}_{n_b}$ follows for example the Rouse equation (98). We present the asymptotic computation of the Mean First Encounter Time (MFET) $\langle \tau_e \rangle$ for the two ends $\boldsymbol{R}_N, \boldsymbol{R}_1$ meets. The two monomers meet when distance is less than $\varepsilon < b$, that is

$$|\boldsymbol{R}_N - \boldsymbol{R}_1| \leqslant \varepsilon \tag{114}$$

In Rouse coordinates, $\boldsymbol{u_p} = \sum_{n=1}^N \alpha_p^n \boldsymbol{R}_n$ where α_p^n are defined in (102), condition (114) is

$$\left| 2\sqrt{\frac{2}{N}} \sum_{p \text{ odd}} \boldsymbol{u}_p \cos(p\pi/2N) \right| \leqslant \varepsilon. \tag{115}$$

The end-to-end encounter is independent of the center of mass, with coordinate $\boldsymbol{u}_0$. Thus, the MFET is the MFPT for the $(N-1)d$-dimensional stochastic process

$$\boldsymbol{u}(t) = (\boldsymbol{u}_1(t), .. \boldsymbol{u}_{N-1}(t)) \in \Omega \times \Omega ... \times \Omega = \tilde{\Omega}, \tag{116}$$

where $\Omega = \mathbb{R}^2$ or $\mathbb{R}^3$ and $\boldsymbol{u}_p$ satisfies the OU-equations (105) to the boundary of the domain

$$S_\epsilon = \{P \in \tilde{\Omega} \text{ such that } \text{dist}(P, \mathcal{S}) \leqslant \frac{\varepsilon}{\sqrt{2}}\}, \tag{117}$$

where *dist* is the Euclidean distance and

$$\mathcal{S} = \{(\boldsymbol{u}_1, .. \boldsymbol{u}_{N-1}) \in \tilde{\Omega} \left| \sum_{p \text{ odd}} \boldsymbol{u}_p \cos(p\pi/2N) = 0\right.\} \tag{118}$$

is a submanifold of codimension d in $\tilde{\Omega}$. The probability density function (pdf) $p(\boldsymbol{u}(t) = \boldsymbol{x}, t)$ satisfies the forward Fokker–Planck equation (FPE) [18]

$$\frac{1}{D} \frac{\partial p(\boldsymbol{x}, t)}{\partial t} = \Delta p(\boldsymbol{x}, t) + \nabla \cdot (\nabla \phi \, p(\boldsymbol{x}, t)) = \mathcal{L}p, \tag{119}$$
$$p(\boldsymbol{x}, 0) = p_0(\boldsymbol{x}),$$

with boundary condition $p(\boldsymbol{x}, t) = 0$ for $x \in \partial S_\epsilon$, $p_0(\boldsymbol{x})$ is the initial distribution and the potential $\phi(u_1, .., u_N) = \frac{1}{2} \sum_p \kappa_p \boldsymbol{u}_p^2$ was introduced in (103).

The solution of equation (119) is expanded in eigenfunctions

$$p(\boldsymbol{x}, t) = \sum_{i=0}^\infty a_i w_{\lambda_i^\epsilon}(\boldsymbol{x}) \mathrm{e}^{-\lambda_i^\epsilon tD} \mathrm{e}^{-\phi(\boldsymbol{x})}, \tag{120}$$

where a_i are coefficients, $w_{\lambda_i^\epsilon}(\boldsymbol{x})$ and λ_i^ϵ are the eigenfunctions and eigenvalues respectively of the operator $\mathcal{L}$ in the domain $\Omega_\epsilon = \tilde{\Omega} - S_\epsilon$. The probability distribution that the two ends have not met before time t is the survival probability

$$p(t) = Pr\{\tau_\epsilon > t\} = \int_{\Omega_\epsilon} p(\boldsymbol{x}, t)\mathrm{d}x, \tag{121}$$

and the first looping time is

$$\tau_\epsilon = \inf\{t > 0, \boldsymbol{u}(t) \in \partial S_\epsilon\}. \tag{122}$$

Using expansion (120), $p(t) = 4\sum_{i=0}^{\infty} C_i \mathrm{e}^{-\lambda_i^\epsilon D t}$ where $C_i = \int_{\Omega_-} p_0(\boldsymbol{x}) w_{\lambda_i^\epsilon}(\boldsymbol{x})\mathrm{d}\boldsymbol{x} \int_{\Omega_\epsilon} w_{\lambda_i^\epsilon}(\boldsymbol{x})\mathrm{e}^{-\phi(\boldsymbol{x})}\mathrm{d}\boldsymbol{x}$. Starting with an equilibrium distribution $p_0(\boldsymbol{x}) = |\tilde{\Omega}|^{-1}\mathrm{e}^{-\phi(\boldsymbol{x})}$, we have

$$C_i = |\tilde{\Omega}|^{-1}(\int_{\Omega_\epsilon} w_{\lambda_i^\epsilon}(\boldsymbol{x})\mathrm{e}^{-\phi(\boldsymbol{x})}\mathrm{d}\boldsymbol{x})^2$$

and finally the MFET is given by

$$\langle \tau_\epsilon \rangle = \sum_{i=0}^{\infty} \frac{C_i}{D\lambda_i^\epsilon}. \tag{123}$$

Starting from the equilibrium distribution $C_0 \approx 1$, while the other terms are $C_i = o(1)$, as we shall see, the first term is the main contributor of the series.

6.3. Computing the eigenvalues of the Fokker–Planck equation and the MFET

The eigenvalues λ_i^ϵ of the operator $\mathcal{L}$ (equation (119)) are obtained by solving the forward FPE in $\mathbb{R}^{d(N-1)}$, with the zero absorbing boundary condition on the entire boundary of the domain S_ϵ (see equation (117)), which is the tubular neighborhood of the $(N-1)d$-dimensional sub-manifold $\mathcal{S}$. For small ε, the eigenvalues can be computed from the following regular expansion near the solution of the domain with no domain S_ϵ:

$$\lambda_i^\epsilon = \lambda_i^0 + c_2\epsilon \int_S w_{\lambda_i^0}^2 \mathrm{d}V_x + \mathcal{O}(\epsilon^2), \text{ for } d = 3 \tag{124}$$

$$\lambda_i^\epsilon = \lambda_i^0 + \frac{2\pi}{\log \epsilon} \int_S w_{\lambda_i^0}^2 \mathrm{d}V_x + \mathcal{O}\left(\left(\frac{1}{\log \epsilon}\right)^2\right) \text{ for } d = 2, \tag{125}$$

where the eigenfunction $w_{\lambda_i^0}$ and eigenvalues λ_i^0 are associated to the non perturbed operator (no boundary) [71], $d = 3, 2$.

In the context of the Rouse polymer, the volume element is $\mathrm{d}V_x = \mathrm{e}^{-\phi(\boldsymbol{x})}\mathrm{d}\boldsymbol{x}_g, \mathrm{d}\boldsymbol{x}_g$, a measure over the sub-manifold $\mathcal{S}$ and $c_2 = \frac{2\pi^{3/2}}{\Gamma(3/2)}$ [71]. The unperturbed eigenfunctions $w_{\lambda_i^0}$ are products of Hermite polynomials [72], that depend on the spatial coordinates and the eigenvalues λ_i^0 are the sum of one dimensional eigenvalues [73]. The first eigenfunction associated to the zero eigenvalue is $w_{\lambda_0^0} = |\tilde{\Omega}|^{-1/2}$. The first eigenvalue for ε small is obtained from relation (124) in dimension 3 with $\lambda_i^0 = 0$,

$$\lambda_0^\epsilon = \frac{c_2\epsilon \int_S \mathrm{e}^{-\phi(\boldsymbol{x})}\mathrm{d}\boldsymbol{x}_g}{|\tilde{\Omega}|} + \mathcal{O}(\epsilon^2), \tag{126}$$

which is the ratio of the closed to all polymer configurations. Using the potential ϕ (defined in (103)), the volume is computed explicitly from Gaussian integrals

$$|\tilde{\Omega}| = \int_\Omega e^{-\phi(x)} dx_g = \left[\frac{(2\pi)^{(N-1)}}{\prod_1^{N-1} \kappa_p} \right]^{d/2}, \tag{127}$$

while the parametrization of the constraint (118) leads to

$$\int_S e^{-\phi(x)} dx_g = \left[\frac{(2\pi)^{N-2} \prod_{p \text{ odd}} \omega_p^2}{\prod_p \kappa_p \left(\sum_{p \text{ odd}} \frac{\omega_p^2}{\kappa_p} \right)} \right]^{d/2}, \tag{128}$$

where $\omega_p = \cos(p\pi/2N)$. In summary, for fix N and small ε,

$$\lambda_0^\epsilon = \begin{cases} \left(\dfrac{\kappa}{N\pi} \right)^{3/2} 4\pi\epsilon + \mathcal{O}(\epsilon^2) & \text{for } d = 3, \\[4mm] \dfrac{2\kappa}{N \log\left(\frac{\sqrt{2}b}{\varepsilon} \right)} + \mathcal{O}\left(\left(\dfrac{1}{\log \epsilon} \right)^2 \right) & \text{for } d = 2. \end{cases} \tag{129}$$

The zero eigenvalue is sufficient to characterize the MFET, confirming that the FET is almost Poissonian, except for very short time. Moreover, the second term in the expansion of λ_0^ϵ is proportional to $1/N$. Using the approximation $C_0 \sim 1$ and relation (123), for $d = 3$, the MFET is approximated by

$$\langle \tau_\varepsilon \rangle_{3d} \approx \frac{1}{D\lambda_0^\epsilon} = \frac{1}{D\left(\left(\frac{\kappa}{N\pi} \right)^{3/2} 4\pi\epsilon - A\epsilon^2/N \right)}, \tag{130}$$

where A is a constant that has been estimated numerically. Indeed, with $\epsilon = \frac{\varepsilon}{\sqrt{2}}$, the MFET is for d = 3

$$\langle \tau_\varepsilon \rangle_{3d} = \left(\frac{N\pi}{\kappa} \right)^{3/2} \frac{\sqrt{2}}{D4\pi\varepsilon} + A_3 \frac{b^2}{D} N^2 + \mathcal{O}(1), \tag{131}$$

which hold for a large range of N, as evaluated with Brownian simulations (figure 3). The value of the coefficient is $A_3 = 0.053$ [73] ($A_3 = 0.053b^2/D$). These estimates are obtained for fixed N and small ε.

Similar for $d = 2$, a a two dimensional space, the asymptotic formula for MFET [73] is

$$\langle \tau_\varepsilon \rangle_{2d} = \frac{N}{2D\kappa} \log\left(\frac{\sqrt{2}b}{\varepsilon} \right) + A_2 \frac{b^2}{D} N^2 + \mathcal{O}(1), \tag{132}$$

All these asymptotic expansions are derived for fix N and small ε. However, there should not be valid in the limit N large, although stochastic simulations (figures 3(a) and (b)) shows that the range validity is broader than expected. The exact asymptotic formula for any two monomers inside a polymer chain should be derived. Other scaling laws have been derived in [70].
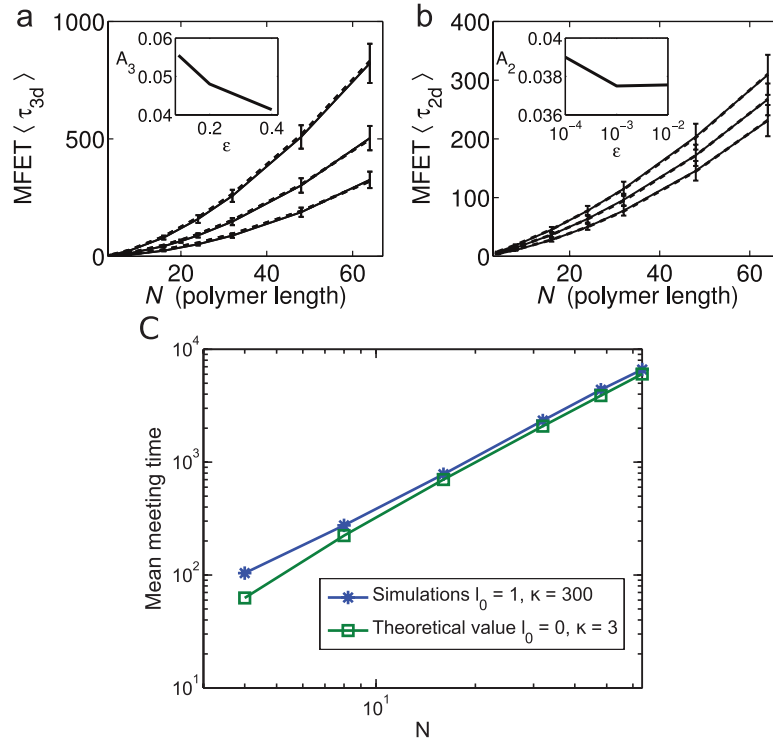
Figure 3. Mean first encounter time (MFET) for different polymer lengths and different values of ε. (a) MFET (three dimensions) estimated from Brownian simulations (full line) and compared to the theoretical MFET (equation (131)) (dashed lines). The parameter A_3 is obtained by fitting ($\varepsilon = 0.1, 0.2, 0.4$). The unit is in b^2/D. (b) The MFET (two dimensions) estimated from Brownian simulation (full lines) and compared to the theoretical MFET (equation (132)) (dashed lines). The parameter A_2 is obtained by fitting ($\varepsilon = 10^{-4}, 10^{-3}, 10^{-2}$) (reproduced from [73]).(c) log–log plot of the MFET in dimension 3.

7. Diffusion approximation by jump processes and model of a membrane crowded with obstacles

Smoluchowski equation has also been used to analyse diffusion in crystal or crowded medium such as cellular membrane. The approach consists of approximating diffusion jump process as continuous diffusion, valid at a much coarser-time scale than the continuous process itself. This approximation allows deriving asymptotic formula and interpreting data [57]. The transition between diffusion at a molecular level and sub-cellular level correspond to changing scale and is obtained by coarse-graining a model of disk obstacles using the narrow escape theory into a Markov process, which is a continuum approximation of the diffusion equation. The transition between the molecular and cellular regime occurs at a time scale characterized by the NET and is often interpreted as anomalous diffusion.

The organization of a cellular membrane is to a large extent the determinant of the efficiency of molecular trafficking of receptors to their destination. The arrival rates of these molecules at their specific destinations control their role and performance, and thus steer the cell
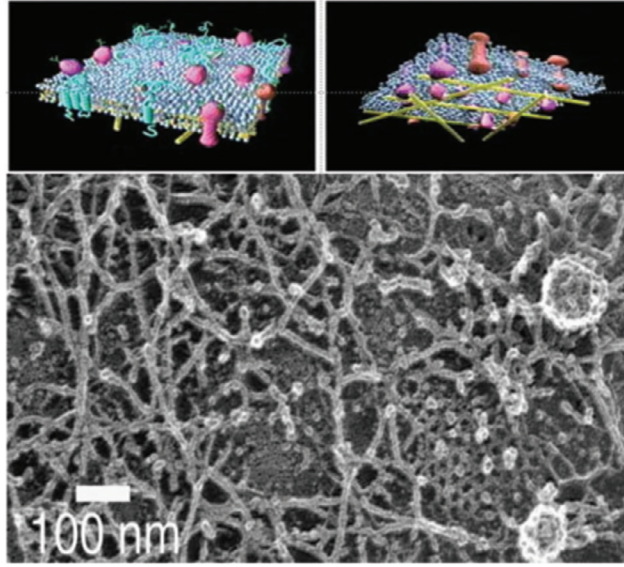
Figure 4. Organization of a neuronal membrane [65] (courtesy of Kusumi) containing microdomains made of overlapping filaments.

toward its function. After two decades of intense research on membrane organization, it is still unclear how the heterogeneity of the membrane controls diffusion (see figure 4). Recently, using single molecule tracking, the diffusion coefficient of a molecule freely diffusing on intact and treated neuronal membranes, cleared of almost all obstacles was found. In this case the diffusion of a protein on the membrane is described by the Saffman–Delbrück theory. If, however, the membrane is crowded with obstacles, such as fixed proteins, fences and pickets, and so on, the effective diffusion coefficient differs significantly from that predicted in and depends strongly on the degree of crowding. The latter can be estimated from diffusion data and from an appropriate model and its analysis, as explained below. The key to assessing the crowding is to estimate the local diffusion coefficient from the measured molecular trajectories and the analytic formula for the MFPT through a narrow passage between obstacles.

7.1. A coarse-grained model of membrane crowding organization

A simplified model of a crowded membrane can be a square lattice of circular obstacles of radius a centered at the corners of lattice squares of side L (figure 5). The mean exit time from a lattice box, formula (82), is to leading order independent of the starting position (x,y) and can be approximated as

$$\bar{\tau}_4 = \frac{\bar{\tau}}{4},\tag{133}$$

where $\bar{\tau}$ is the MFPT to a single absorbing window in a narrow strait with the other windows closed (reflecting instead of absorbing). It follows that the waiting time in the cell enclosed by the obstacles is exponentially distributed with rate

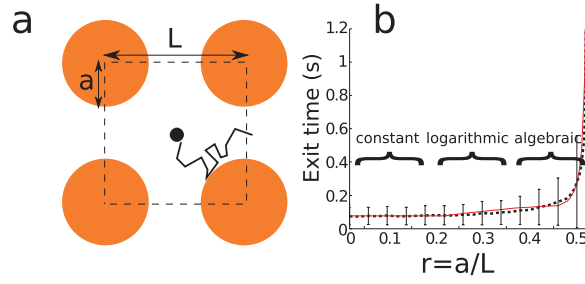$$\lambda = \frac{1}{2\tau_4},\tag{134}$$

Figure 5. NET versus scaled radius of obstacles. NET from the domain (a) with $D = 1$, $L = 1$. Statistics were obtained from 1000 exit times/point of simulated Brownian trajectories (dashed line). (b) NET versus obstacle scaled radius $r = a/L = \frac{1}{2}(1 - \varepsilon)$. The simulated (dotted curve) and analytical approximation (135) (continuous curve) for $0 < r = r_1 = 0.2$, $r_1 < r < r_2 = 0.45$, and $0.45 < r < 0.5$ [15].

where $\bar{\tau}$ is given by (80) and (82) as

$$
\bar{\tau} \approx
\begin{cases}
c_1 \text{ for } 0.8 < \varepsilon < 1, \\[2mm]
c_2 |\Omega| \log \dfrac{1}{\varepsilon} + d_1 \text{ for } 0.55 < \varepsilon < 0.8, \\[2mm]
c_3 \dfrac{|\Omega|}{\sqrt{\varepsilon}} + d_2 \text{ for } \varepsilon < 0.55,
\end{cases}
\tag{135}
$$

with $\varepsilon = (L - 2a)/a$ and $d_1, d_2 = O(1)$ for $\varepsilon \ll 1$ (see figure 5). The MFPT c_1 from the center to the boundary of an unrestricted square is computed from

$$
u(x, y) = \frac{4L^2}{\pi^3 D} \sum_0^\infty \frac{\left[\cosh(k + \frac{1}{2})\pi - \cosh(k + \frac{1}{2})\pi(2y/L - 1)\right] \sin(2k + 1)\pi x/L}{(2k + 1)^3 \cosh(2k + 1)\pi},
\tag{136}
$$

so $c_1 = u(L/2, L/2) \approx [4L^2/\pi^3 D][\cosh(\pi/2 - 1)/\cosh \pi]$. For $L = 1, D = 1$, we find $c_1 \approx 0.076$, in agreement with Brownian dynamics simulations (figure 5(B)). The coefficient c_2 is obtained from (78) as $c_2 = 1/2\pi D \approx 0.16$. Similarly, the coefficient c_3 is obtained from (82) as $c_3 \approx \pi/4\sqrt{2} \, D \approx 0.56$. The coefficients d_i are chosen by patching $\bar{\tau}$ continuously between the different regimes:

$$
d_1 = c_1 + c_2 |\Omega(r_1)| \log(1 - 2r_1),
\tag{137}
$$

and

$$
\begin{aligned}
d_2 = c_1 &- c_2 \big[|\Omega(r_1)| \log(1 - 2r_1) + |\Omega(r_2)| \log(1 - 2r_2)\big] \\
&- c_3 |\Omega(r_2)|(1 - 2r_2)^{-1/2},
\end{aligned}
$$

where $|\Omega(r)| = L^2 - \pi r^2$.

Simulations with $D = 1$ in a square of radius $L = 1$ with four reflecting circles of radius r, centered at the corners, show that the uniform approximation by the patched formula (135) is in good agreement with Brownian results (figure 5(b)), where the statistics were collected from 1000 escape times of Brownian trajectories per graph point. The trajectories start at the square center. Equation (135) holds in the full range of values of $a \in [0, L/2]$ and all L.

The Brownian motion around the obstacles (figure 5(a)) can be coarse-grained into a Markovian jump process whose state are the connected domains enclosed by the obstacles and the jump rates are determined from the reciprocals of the mean first passage times and exit probabilities. This random walk can in turn be approximated by an effective coarse-grained anisotropic diffusion. The diffusion approximation to the transition probability density function of an isotropic random walk that jumps at exponentially distributed waiting times with rate λ on a square lattice with step size L is given by [18]

$$\frac{\partial p}{\partial t} = \bar{D}\left(\frac{\partial^2 p}{\partial x^2} + \frac{\partial^2 p}{\partial y^2}\right), \quad \bar{D} = \frac{\lambda L^2}{4}. \tag{138}$$

7.2. Diffusion of receptors on the neuronal membrane

The results of the previous section can be used to estimate the density of obstacles on the membrane of cell such as a neuronal dendrite. The effective diffusion coefficient of a receptor on the neuronal membrane can be estimated from the experimentally measured single receptor trajectory by a single particle tracking method. The receptor effective diffusion coefficient of a receptor varies between 0.01 and 0.2 μm^2/sec.

In the simplified model of crowding, the circular obstacles are as in (figure 5). Simulated Brownian trajectories give the MFPT from one square to the next one as shown in figure 4, where L is fixed and a is variable. According to (135), (134) and (138), as a increases the effective diffusion coefficient $\bar{D}$ decreases. It is computed as the as the mean square displacement (MSD) $\langle\frac{MSD(t)}{4t}\rangle$. Brownian simulations show that $\bar{D}$ is linear, thus confirming that in the given geometry crowding does not affect the nature of the Brownian motion for sufficiently long times. Specifically, for Brownian diffusion coefficient $D = 0.2$ μm^2 s^{-1} the time considered is longer than 10 s. In addition, figure 6(c) shows the diffusion coefficient ratio D_a/D_0, where D_a is the effective diffusion coefficient of Brownian motion on the square lattice described above with obstacles of radius a. For $a = 0.3$ the value $D_a/D_0 \approx 0.7$ is found whereas a direct computation from the mean exit time formula (135) gives

$$\frac{\tau_0}{\tau_a} = \frac{c_1}{c_2|\Omega|\log\frac{1}{\varepsilon} + d_1} \approx 0.69, \tag{139}$$

where $\varepsilon = (L - 2a)/L = 0.4$.

It can be concluded from the Brownian simulations that the coarse-grained motion is plain diffusion with effective diffusion coefficient $D_a/D_0 = \tau_0/\tau_a$, which decreases nonlinearly as a function of the radius a, as given by the uniform formula (135). Figure 6 recovers the three regimes of (135): the uncrowded regime for $a < 0.2L$, where the effective diffusion coefficient does not show any significant decrease, a region $0.2L < a < 0.4L$, where the leading order term of the effective diffusion coefficient is logarithmic, and for $a > 0.4L$ the effective diffusion coefficient decays as $\sqrt{(L - 2a)/L}$, in agreement with (135).

Finally, to estimate the density of obstacles in a neuron from (135), (134) and (138), a reference density has to be chosen. The reference diffusion coefficient is chosen to be that of receptors moving on a free membrane (with removed cholesterol), estimated to be $0.17 \leqslant D \leqslant 0.2$ μm^2 s^{-1} [14], while with removing actin, the diffusion coefficient is 0.19 μm^2 s^{-1}. The reference value $D = .2$ μm^2 s^{-1} gives an estimate of the crowding effect based on the measured diffusion coefficient (figure 6(d)). The reduction of the diffusion coefficient from $D = 0.2$ μm^2 s^{-1} to $D = 0.04$ μm^2 s^{-1} is achieved when 70% of the membrane surface is occupied

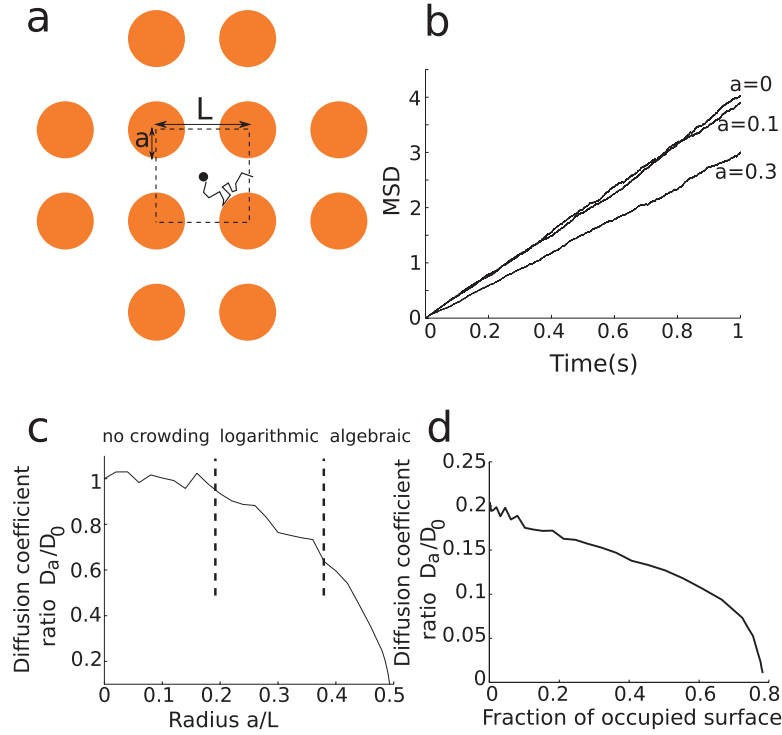J. Phys. A: Math. Theor. **00** (2016) 000000

Topical Review

Figure 6. Organization of the neuronal membrane. (a) Schematic representation of a Brownian particle diffusing in a crowded microdomain. (b) Mean square displacement (MSD) of the particle in a domain paved with microdomains. The MSD is linear, showing that crowding does not affect the nature of diffusion. The effective diffusion coefficient is computed as $\bar{D} = \lim_{t \to \infty} \langle MSD(t)/4t \rangle$ for $D = 1$. (c) The effective diffusion coefficient computed from the MSD for different radiuses of the obstacles. Brownian simulations (continuous curve): there are three regions (separated by the dashed lines). While there is no crowding for $a < 0.2$, the decreasing of the effective diffusion coefficient for $0.2 < a < 0.4$ is logarithmic, and like square root for $a > 0.4$. (d) Effective diffusion coefficient of a particle diffusing in a domain as a function of the fraction of the occupied surface. An AMPAR has a diffusion coefficient of 0.2 μm^2 s^{-1} in a free membrane (reproduced from [15]).

by obstacles. Thus obstacles impair the diffusion of receptors and are therefore responsible for the large decrease of the measured diffusion coefficient (up to 5 times). To conclude, as illustrated in figure 7, diffusion in a crowded membrane involves various time regimes: at very short time scale, before a Brownian particle has the time to escape between small aperture near obstacles, the particle diffuses freely, characterized by the homogeneous membrane diffusion coefficient. This approximation is valid before the NET time scale is reached (see formula (82)). For longer time, $t \gg \bar{\tau}$, the motion of a Brownian particle is characterized again by a diffusion process, but now the diffusion coefficient does account for the obstacles and in the very density limit, the effective diffusion coefficient is given by

$$D_e = D \frac{L^2}{2\pi(L^2 - \pi R^2)} \sqrt{\frac{L - 2R}{R}}, \text{ for } R \leqslant L/2. \tag{140}$$
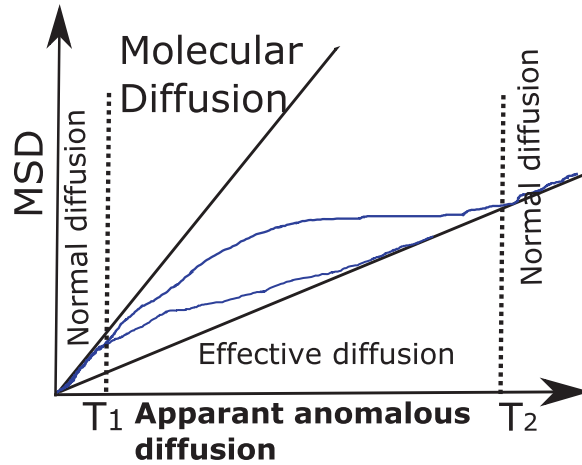
Figure 7. Summary of MSD for diffusion in a crowded membrane. There are two normal diffusion regimes, separated by a transient regime, which exhibits an apparent anomalous diffusion due to the transition between obstacles.

At an intermediate time regime between the two extreme cases described above, a stochastic particle is hopping from one square to another, characterized as anomalous diffusion (blue curves in figure 7).

8. Jump processes for a model of telomere length dynamics

Stochastic jumps are inherent to physical and biological processes that can be studied in various limits (diffusion approximation [18]). We review here the example of a telomere (end of a chromosome) model introduced in [75, 76], in which the length x of the telomere can decrease or increase at each division.

The length x decreases by a fixed length a with probability $l(x)$ or, if recognized by a polymerase, it increases by fixed length b with probability $r(x) = 1 - l(x)$. The jump probability $r(x)$ is a decreasing function of x with $r(0) = 1$. Thus the length of the telomere at division n is an asymmetric random walk $x(n)$. In this simplified model, the maximal length of a telomere is $L \gg b$. When the length falls below a critical value T, cell division stops.

8.1. The asymmetric random jump model

The model of the telomere dynamics is

$$x_{n+1} = \begin{cases} x_n - a & \text{w.p. } l(x_n) \\ x_n + b & \text{w.p. } r(x_n), \end{cases} \tag{141}$$

where the right-probability $r(x)$ can be approximated by

$$r(x) = \frac{1}{1 + \alpha x}, \tag{142}$$

for some $\alpha > 0$. Scaling $x_n = y_n L$ and setting $\varepsilon = b/L$, the dynamics (141) becomes

$$
y_{n+1} = \begin{cases} y_n - \dfrac{\varepsilon a}{b} & \text{w.p. } \tilde{l}(y_n) \\ y_n + \varepsilon & \text{w.p. } \tilde{r}(y_n), \end{cases} \tag{143}
$$

where $\tilde{l}(y) = l(x)$ and $\varepsilon T/b < y < 1$. In the limit $\varepsilon \ll 1$, the process y_n moves in small steps. The dynamics (143) falls under the general scheme (see [18])

$$
y_{n+1} = y_n + \varepsilon \xi_n, \tag{144}
$$

where

$$
\Pr\{\xi_n = \xi \mid y_n = y, y_{n-1} = y_1, \ldots\} = w(\xi \mid y, \varepsilon), \tag{145}
$$

ε is a small parameter, and y_0 is a random variable with a given pdf $p_0(y)$. In the case at hand the function $w(\xi \mid y)$ defined in (145) is given by

$$
w(\xi \mid y) = (1 - \tilde{r}(y))\delta\!\left(\xi + \frac{a}{b}\right) + \tilde{r}(y)\delta(\xi - 1), \tag{146}
$$

The pdf of y_n satisfies the backward equation for $0 < x < 1$

$$
p_\varepsilon(y, n \mid x, m) - p_\varepsilon(y, n \mid x, m + 1)
$$
$$
= p_\varepsilon\!\left(y, n \mid x - \varepsilon\frac{a}{b}, m + 1\right)\tilde{l}(x) + p_\varepsilon(y, n \mid x + \varepsilon, m + 1)\tilde{r}(x) - p_\varepsilon(y, n \mid x, m). \tag{147}
$$

The first conditional jump moment, $m_1(y) = -a\tilde{l}(y)/b + \tilde{r}(y)$ changes sign at $z_0 = b/L\alpha a$, so $p_\varepsilon(y, n)$ converges to a quasi-stationary density $p_\varepsilon(y)$ for large n, before the trajectory y_n is terminated at $y = T/L$.

One dimensional processes (see equation (144)) in the small jump limit is described in [18] p 236 and p 303, see also [79–81]. In this limit, the Kramers–Moyal approximation consists in expanding in ε and then approximating equation (147) by a direct truncation to a second order equation. The method is equivalent to construct a stochastic processes with the first and second moments that match the coefficients of the Kramers–Moyal approximation. We present below the WKB construction of an approximated solution.

8.2. Construction of the quasi steady-state density $p_\varepsilon(y)$

The structure of the quasi-stationary solution $p_\varepsilon(y)$ for $\varepsilon \ll 1$ and $y > \varepsilon$, can be obtained in the WKB form [18]

$$
p_\varepsilon(y) = K_\varepsilon(y)\exp\left\{-\frac{\psi(y)}{\varepsilon}\right\}, \tag{148}
$$

where

$$
K_\varepsilon(y) = \sum_{i=0}^{\infty} \varepsilon^i K_i(y) \tag{149}
$$

and $K_i(y)$ are chosen such that $p_\varepsilon(y)$ is normalized. The components of the expansion (148) are found by solving the eikonal equation for $\psi(y)$

$$
\int_{\mathbb{R}} [e^{\xi\psi'(y)} - 1]\, w(\xi \mid y, 0)\, d\xi = 0, \tag{150}
$$

which for the problem at hand takes the form

$$\tilde{l}(y)\exp\left\{-\psi'(y)\frac{a}{b}\right\} + \tilde{r}(y)\exp\{\psi'(y)\} = 1 \text{ for } y > \varepsilon. \tag{151}$$

At the next order in ε, we find that $K_0(y)$ is the solution of the 'transport' equation

$$\int_{\mathbb{R}}\left\{\frac{\partial}{\partial y}[w(\xi\mid y)K_0(y)] + \frac{\xi w(\xi\mid y)}{2}\psi''(y)K_0(y)\right\}\xi e^{\xi\psi'(y)}\,d\xi = 0. \tag{152}$$

Equation (152) has a removable singularity at $y = z_0$, because the coefficient of K_{0y} in (152),

$$\int_{\mathbb{R}}\xi w(\xi\mid y)e^{\xi\psi'(y)}\,d\xi = \int_{\mathbb{R}}\xi w(\xi\mid y)[1 + \xi\psi''(z_0)(y - z_0) + O((y - z_0)^2)]\,d\xi$$
$$= [m_1'(z_0) + m_2(z_0)\psi''(z_0)](y - z_0) + O((y - z_0)^2)$$
$$= -m_1'(z_0)(y - z_0) + O((y - z_0)^2),$$

vanishes linearly at z_0. However, the coefficient of $K_0(y)$ in (152) also vanishes at z_0.

8.3. Extreme statistics for the shortest telomere

In this section, we present a different approach for computing the steady solution of the pdf for the process (141). We derive the Takacs equation and then study the statistics of the shortest trajectory (shortest telomere) for an ensemble of n identical independently distributed (iid) processes.

The steady state distribution associated to the telomere equation (141) can be rescaled with a constant drift for shortening, and possible large jumps with exponential rates for elongation. The jump rate function becomes $\lambda(X) = \frac{1}{1 + BX}$, and the probability for the jump $\bar{\xi}$ is given by $Pr(\bar{\xi} = y) = \theta e^{-\theta y} = b(y)$, where $B = a\beta$ and $\theta = ap$. The pdf $f(x, t) = \partial F(x, t)/\partial x$ where $F(x, t) = \Pr\{X(t) \leqslant x\}$ satisfies the Takacs equation, which is written for the forward Fokker–Planck equation $x > 0$,

$$\partial_t f = \partial_x f - \lambda(x)f(x, t) + \int_0^l \lambda(y)f(y, t)b(x - y)\,dy. \tag{153}$$

The stationary distribution function is [76]

$$\bar{f}(x) = \frac{\theta\left[\theta(x + \frac{1}{B})\right]^{\frac{1}{B}} e^{-\theta\left(x + \frac{1}{B}\right)}}{\Gamma\left(\frac{1}{B} + 1, \frac{\theta}{B}\right)}, \tag{154}$$

where $\Gamma(s, x) = \int_x^{+\infty} t^{s-1}e^{-t}\,dt$ is the upper incomplete Gamma function. Now the distribution of the shortest telomere [76] in an ensemble of $2n$ telomeres, corresponding to a total of n chromosomes (16 in yeast and n is in the range of 36–60) is estimated when their lengths are independent identically distributed variables $L_1, L_2, \ldots L_{2n}$. Considering $2n$ iid variables $X_1, \ldots X_{2n}$ following a distribution f, the pdf of the minimum $X_{(1:2n)} = \min(X_1, X_2, \ldots X_{2n})$ is given by

$$f_{X_{(1:2n)}}(x) = 2n(1 - F)^{2n-1}(x)f(x), \tag{155}$$

where $F(x) = \int_0^x f(u)du$. The statistical moments $\bar{X}_{(1:2n)}^k = \int_{\mathbb{R}+} x^k f_{X_{(1:2n)}}(x)\,dx$ are given by

$$\bar{X}_{(1:2n)}^k = k \int_{\mathbb{R}+} x^{k-1}(1 - F)^{2n}(x)\mathrm{d}x. \tag{156}$$

When f is a Gamma distribution of parameter α and n sufficiently large, $\bar{X}_{(1:2n)}^k$ can be estimated using the Laplace's method.

In the limit x tends to 0, equation (154) with $\alpha = 1 + \frac{1}{B}$ satisfies $F(x) \approx mx^r$ with $m = \frac{1}{\alpha\Gamma(\alpha)} > 0$ and $r = \alpha > 1$,

$$\bar{X}_{(1:2n)}^k = \frac{k}{r} \int_0^{+\infty} x^{k/r-1} \exp[2n \ln(1 - F(x^{1/r}))]\mathrm{d}x \approx \bar{X}_{(1:2n)}^k \approx \frac{k\Gamma\left(\frac{k}{\alpha}\right)}{\alpha}\left(\frac{\alpha\Gamma(\alpha)}{2n}\right)^{k/\alpha}. \tag{157}$$

Using formulae (155)–(157), the pdf and the moments of the shortest telomere length $L_{1:2n}$ for $k = 1$ can be estimated and the shortest telomere length is

$$\bar{L}_{(1:2n)} \approx L_0 - \frac{1}{B} + \frac{\Gamma\left(1 + \frac{1}{B}\right)\Gamma\left(\frac{1}{1+1/B}\right)^{\frac{1}{1+1/B}}}{p\left(1 + \frac{1}{B}\right)^{\frac{1}{1+B}}(2n)^{\frac{1}{1+1/B}}}. \tag{158}$$

Using the values $p = 0.026$, $\beta = 0.045$ ($B = 0.16 < 0.5$) and $L_0 = 90$ (yeast) and equation (156) for $k = 1$ and 2, the mean shortest telomere length is 184 ± 25 bps.

To estimate the gap between the shortest telomere and the others, we shall compute the distribution of the second shortest length $X_{(2:2n)}$. The pdf $f_{X_{(2:2n)}}$ of $X_{(2:2n)}$ is given by

$$f_{X_{(2:2n)}}(x) = 2n(2n - 1)F(x)(1 - F(x))^{2n-2}f(x), \tag{159}$$

and the statistical moments $\bar{X}_{(2:2n)}^k$ satisfy the induction relation

$$\bar{X}_{(2:2n)}^k = n\bar{X}_{(1:2n-1)}^k - (2n - 1)\bar{X}_{(1:2n)}^k. \tag{160}$$

Using equation (157) for $k = 1$, we obtain that the ratio $\frac{\bar{X}_{(2:2n)}}{\bar{X}_{(1:2n)}}$, for n or $B \gg 1$ is given asymptotically for $\alpha = 1 + \frac{1}{B}$ by

$$\frac{\bar{X}_{(2:2n)}}{\bar{X}_{(1:2n)}} \approx 1 + \frac{1}{\alpha}. \tag{161}$$

To conclude, for a pdf with a nonzero first order derivative at 0, this ratio is a universal number $\frac{3}{2}$. In the case of yeast, equation (160) reveals that the mean length of the second shortest telomere is 207 bps. Thus, the shortest telomere is on average 22 bps shorter than the second one. This gap results from the statistical property of the telomere number and dynamics and should exist in all species. It suggests that the length of the shortest telomere controls the number of division. The computation of the mean time to threshold is more involved as it requires finding an approximation of the pdf in two time intervals. Interestingly, this time depend on the escape of a coarse-grained stochastic dynamics from an effective potential [84].

9. Hybrid discrete-continuum modeling for stochastic gene expression within a autoregulatory positive feedback loop

We end this tribute to Smoluchowski by a description of stochastic modeling of gene activation and regulation. The difficulty in such modeling is the presence of the continuum and discrete
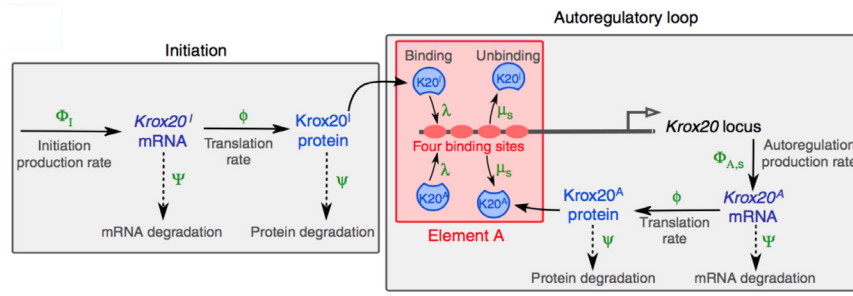
Figure 8. Representation of Krox20 expression in two phases: a first phase lasts for t_I minutes and the production involves both a Krox20-independent initiation process and the autoregulatory loop, whereas only autoregulation is maintained afterwards [85].

description to account for few mRNA (discrete) and large synthesized proteins (continuum). Gene expression is often model by classical Mass-Action laws with additive noise. We present here an alternative approach based on Markov jump processes and we the large number approximation to simplify the equation. The result is a hybrid continuum-discrete ensemble of equations that can give different predictions than classical model. The model is applied to a positive feedback loop of gene regulation based on a transcription factor called Krox20 [85].

We recall that proteins are produced by mRNAs. Sometimes such mechanism involves a feedback control of the proteins on the gene to regulate the mRNA production. For a positive feedback, the produced proteins bind the gene sites to activate the mRNA production. A transcription factor such as Krox20 positively regulates its own expression and results in a bistable switch: either proteins are expressed or not. The model is also used to extract parameters from data and predict the level of expression inside a cell population. Krox20 is involved in the hindbrain anterior-posterior identity, where 7–8 segments called rhombomeres are formed and the transcription factor is required for the particular construction of rhombomeres 3 and 5. The stochastic model of Krox20 expression is based on the interaction between mRNA and proteins, cooperative binding/unbinding of Krox20 proteins to four binding sites on the DNA called A (figure 8). The difficulty in such a model is that only a few mRNA molecules are involved in the activation process, which is coupled to a continuous description of proteins.

9.1. Stochastic model of gene activation

To compute the number of proteins, we need to follow simultaneously three variables: the state s of element A, the number m of *Krox20* mRNA and the number n of unbound Krox20 proteins. The joint probability $p_s(m,n,t)$ to find element A in state s with m *Krox20* mRNA molecules and n free Krox20 proteins is

$$p_s(m,n,t) = Pr\{s(t) = s, mRNA(t) = m, Krox20(t) = n\} \tag{162}$$

and it satisfies a Master equation [18], where only one binding or unbinding occurs at a time

$$\frac{\partial p_s}{\partial t}(m,n,t) = \Phi_s p_s(m-1,n,t) + (m+1)\Psi p_s(m+1,n,t) - (\Phi_s + m\Psi)p_s(m,n,t)$$
$$+ m\phi p_s(m,n-1,t) + (n+1)\psi p_s(m,n+1,t) - (m\phi + n\psi)p_s(m,n,t)$$
$$+ \mu_{s+1}p_{s+1}(m,n-1,t) + (n+1)\lambda_{s-1}p_{s-1}(m,n+1,t) - (\mu_s + n\lambda_s)p_s(m,n,t). \tag{163}$$

The mRNA production rate is given function

$$\Phi_s(t) = \Phi_I \theta(t_I - t) + \Phi_{A,s} \tag{164}$$

where $\theta(t)$ is the Heaviside function. There function models an initial phase where proteins are produced until time t_I. During this phase, mRNA is produced with a Poissonian rate Φ_I by an external molecule. Each mRNA protein is degraded with a Poissonian rate Ψ. Proteins are produced with a Poissonian rate ϕ and are degraded with a rate ψ and can bind to a promoter site that has $N_b = 4$ binding sites. The state of A is characterized by $s = 0, 1, 2, 3, 4$ bound molecules. The autoregulatory production of mRNA occurs with Poissonian rates $\Phi_{A,s} = \Phi_A \xi_s$ that depend on state s, where Φ_A is the maximal production rate and ξ_s describes the modulation due to the state of element A. Binding and unbinding of proteins to A are described by state dependent binding and unbinding rates λ_s and μ_s.

When the change in the number of free Krox20 proteins n due to binding and unbinding to element A is neglected, in the limit $n \gg N_b$, the Master equation (163) can be approximated by

$$
\begin{aligned}
\frac{\partial p_s}{\partial t}(m,n,t) =\ & \Phi_s p_s(m-1,n,t) + (m+1)\Psi p_s(m+1,n,t) - (\Phi_s + m\Psi)p_s(m,n,t) \\
& + m\phi p_s(m,n-1,t) + (n+1)\psi p_s(m,n+1,t) - (m\phi + n\psi)p_s(m,n,t) \\
& + \mu_{s+1}p_{s+1}(m,n,t) + n\lambda_{s-1}p_{s-1}(m,n,t) - (\mu_s + n\lambda_s)p_s(m,n,t)
\end{aligned}
\tag{165}
$$

The first line in equation (165) describes the production and degradation of a mRNA, while the second is for the production and degradation of a Krox20 protein. The last one is for the binding and unbinding of a Krox20 protein to element A. The marginal probabilities is

$$p_s(m,n,t) = \sum_{s'=0}^{N_b} p_{s,s'}(m,n,t) = \sum_{s'=0}^{N_b} p_{s',s}(m,n,t). \tag{166}$$

Binding and unbinding to element A is fast compared to the turn over of proteins, thus we use the approximation

$$p_s(m,n,t) \approx p(m,n,t)p_s(n), \tag{167}$$

where $p_s(n)$ are the steady-state probabilities to find element A in state s for a given number of Krox20 proteins n, and $p(m,n,t)$ is the probability to find m mRNA molecules and n proteins at time t.

The steady state condition for binding and unbinding from equation (165) is

$$\mu_{s+1}p_{s+1}(n) = n\lambda_s p_s(n), \tag{168}$$

leading to the solution

$$p_s(n) = \frac{\prod_{j=0}^{s-1} n\gamma_j}{\sum_{i=0}^{N_b} \prod_{j=0}^{i-1} n\gamma_j}, \tag{169}$$

where

$$\gamma_i = \frac{\lambda_i}{\mu_{i+1}}, \quad i = 0, \dots N_b - 1. \tag{170}$$

The effective mRNA production rates is defined by

$$\Phi_A(n) = \sum_{s=0}^{N_b} \Phi_{A,s} p_s(n) = \Phi_A \sum_{s=0}^{N_b} \xi_s p_s(n). \tag{171}$$

At this stage, the approximated Master equation for the joint pdf $p(m,n,t)$ is

$$\frac{\partial p_s}{\partial t}(m,n,t) = = \Phi(n,t)p(m-1,n,t) + (m+1)\Psi p(m+1,n,t) - (\Phi(n,t)+m\Psi)p(m,n,t)$$
$$+ m\phi p(m,n-1,t) + (n+1)\psi p(m,n+1,t) - (m\phi + n\psi)p(m,n,t) \tag{172}$$

The marginal probabilities for mRNA molecules, Krox20 proteins and the state of element A are

$$p(m,t) = \sum_{s=0}^{N_b} \sum_{n=0}^{\infty} p_s(m,n,t) = \sum_{n=0}^{\infty} p(m,n,t),$$
$$p(n,t) = \sum_{s=0}^{N_b} \sum_{m=0}^{\infty} p_s(m,n,t) = \sum_{m=0}^{\infty} p(m,n,t),$$
$$p_s(t) = \sum_{m=0}^{\infty} \sum_{n=0}^{\infty} p_s(m,n,t) = \sum_{n=0}^{\infty} p(n,t)p_s(n). \tag{173}$$

It remains difficult to study equations (172) because n can be large while m is of the order of few and thus there is no clear limit approximations. The long-time asymptotic is however an important quantity to estimate and in particular how it depends on initial conditions. This limit tells us whether or not a cell expresses Krox20. The diffusion approximation leads to a dynamical system that predicts a two state attractors characterized by full or zero expression, while the Master system shows that there is be a continuum level of expression, but the distribution is dominated by two peaks. This difference justifies the need of a Markov chain description, in particular to study cells at the boundary between regions, where a graded expression is predicted.

9.2. Mean-field approximation

The mean field approximation for the mean quantities is based on the scaled variables

$$\tau = \Psi t, \quad \hat{m} = \frac{m}{m_0}, \quad \hat{n} = \frac{n}{n_0} \tag{174}$$

and the normalized parameters are

$$m_0 = \frac{\Phi_A}{\Psi}, \quad n_0 = m_0 \frac{\phi}{\psi}, \quad \alpha = \beta n_0, \quad \epsilon = \frac{\Psi}{\psi}, \quad \chi = \frac{\Phi_I}{\Phi_A}, \tag{175}$$

where the average values m_0 and n_0 characterize the mRNA and proteins when element A is fully activated. The mean-field equation in the scaled variables $\hat{m}$ and $\hat{n}$ is expressed using the function

$$f(x) = \sum_{s=0}^{N_b} \xi_s \frac{\prod_{j=0}^{s-1} x\tilde{\gamma}_j}{\sum_{i=0}^{N_b} \prod_{j=0}^{i-1} x\tilde{\gamma}_j}. \tag{176}$$

Indeed, the Kramers–Moyal expansion of equation (172) is

$$\frac{\partial p(\hat{m}, \hat{n}, \tau)}{\partial \tau} = \sum_{k=1}^{\infty} \left(\frac{1}{m_0}\right)^{k-1} \frac{\partial_{\hat{m}}^k}{k!} ((-1)^k (\chi \theta(\tau_I - \tau) + f(\alpha \hat{n})) + \hat{m}) p(\hat{m}, \hat{n}, \tau)$$

$$+ \frac{1}{\epsilon} \sum_{k=1}^{\infty} \left(\frac{1}{n_0}\right)^{k-1} \frac{\partial_{\hat{n}}^k}{k!} ((-1)^k \hat{m} + \hat{n}) p(\hat{m}, \hat{n}, \tau) \qquad (177)$$

From truncating the series at first order and neglecting the initiation ($\chi = 0$), we obtain the first order dynamical system, which is the mean-field equation [18]:

$$\begin{aligned}
\frac{d}{d\tau} \hat{m} &= \chi \theta(\tau_I - \tau) + f(\alpha \hat{n}) - \hat{m} \\
\frac{d}{d\tau} \hat{n} &= \frac{1}{\epsilon} (\hat{m} - \hat{n}).
\end{aligned} \qquad (178)$$

The fixed points are given by $\hat{n}^* = \hat{m}^*$ in equation (178). When $\chi = 0$, there is a minimal value $\alpha_{\min} \approx 33.8$ for which $\alpha < \alpha_{\min}$, there is a single fixed point $\hat{m}^* = 0$ ($\alpha_{\min}$, computed using the solution z_0 of $\frac{f'(x)}{f(x)} = \frac{1}{x}$. The minimum value is $\alpha_{\min} = \frac{z_0}{f(z_0)} = \frac{1}{f'(z_0)}$).

For $\alpha > \alpha_{\min}$, there are two stable fixed points $\hat{m}_1^*$ and $\hat{m}_3^*$ and an unstable saddle point $\hat{m}_2^*$ (figure 9 Upper). For large α, the asymptotic values are $\hat{m}_2^* \to 0$ and $\hat{m}_3^* \to 1$. The value $\hat{m}_3^* \approx 1$ ($m_3^* = m_0 \hat{m}_3^* \approx \frac{\phi_A}{\Psi}$) corresponds to the situation where element A is fully activated (figure 9).

The two stable fixed points defines two basins of attraction and a saddle point for $\alpha > \alpha_{\min}$, contained in a separatrix (figure 9 Upper for $\alpha = 40$). For an initial conditions outside the basin of attraction of the fixed point $\hat{m}_1^*$, the dynamics evolves towards the Up attractor (a high protein expression level). In contrast, for a small amplitude initiation, the expression vanishes. In figure 9 (Upper left) shows the separatrix for different values of α: with increasing α the basin of attraction of $\hat{m}_1^* = 0$ shrinks and asymptotically vanishes for large α. In summary, the mean field dynamical system underlying protein activation shows a bistable behavior between two attractors depending on the initial condition, which can be seen as a random variable In contrast, the numerical analysis of the Master equation (172) for the probability $p(m,n,t)$ with the scaled variables $\hat{m}$ and $\hat{n}$, $p(\hat{m}, \hat{n}, t)$ for $p(m,n,t)$ uses the marginal probabilities defined in equation (173). The mean values for $\hat{m}$ and $\hat{n}$ are given by

$$\begin{aligned}
\bar{\bar{m}}(t) &= \frac{1}{m_0} \sum_{n=0}^{\infty} m p(m,n,t) = \frac{1}{m_0} \sum_{m=0}^{\infty} m p(m,t) = \frac{\bar{m}(t)}{m_0}, \\
\bar{\bar{n}}(t) &= \frac{1}{n_0} \sum_{m,n=0}^{\infty} n p(m,n,t) = \frac{1}{n_0} \sum_{n=0}^{\infty} n p(n,t) = \frac{\bar{n}(t)}{n_0}
\end{aligned} \qquad (179)$$

In [85], the analysis reveals that for $\beta > 0.13$ the probability distribution $p(\hat{n})$ at time $t = 500$ min is bimodal with peaks at zero and close to one (figure 9 Lower panel). To conclude, simulating the Master equations reveals a continuum of steady state characterized by two peaks, while the mean field approximation predict a bistable distribution, where the dynamics can fall into one of two attractors. More stochastic analysis is expected to reveal in the future how gene expression regulate development, boundary between brain regions [86] or diseases.
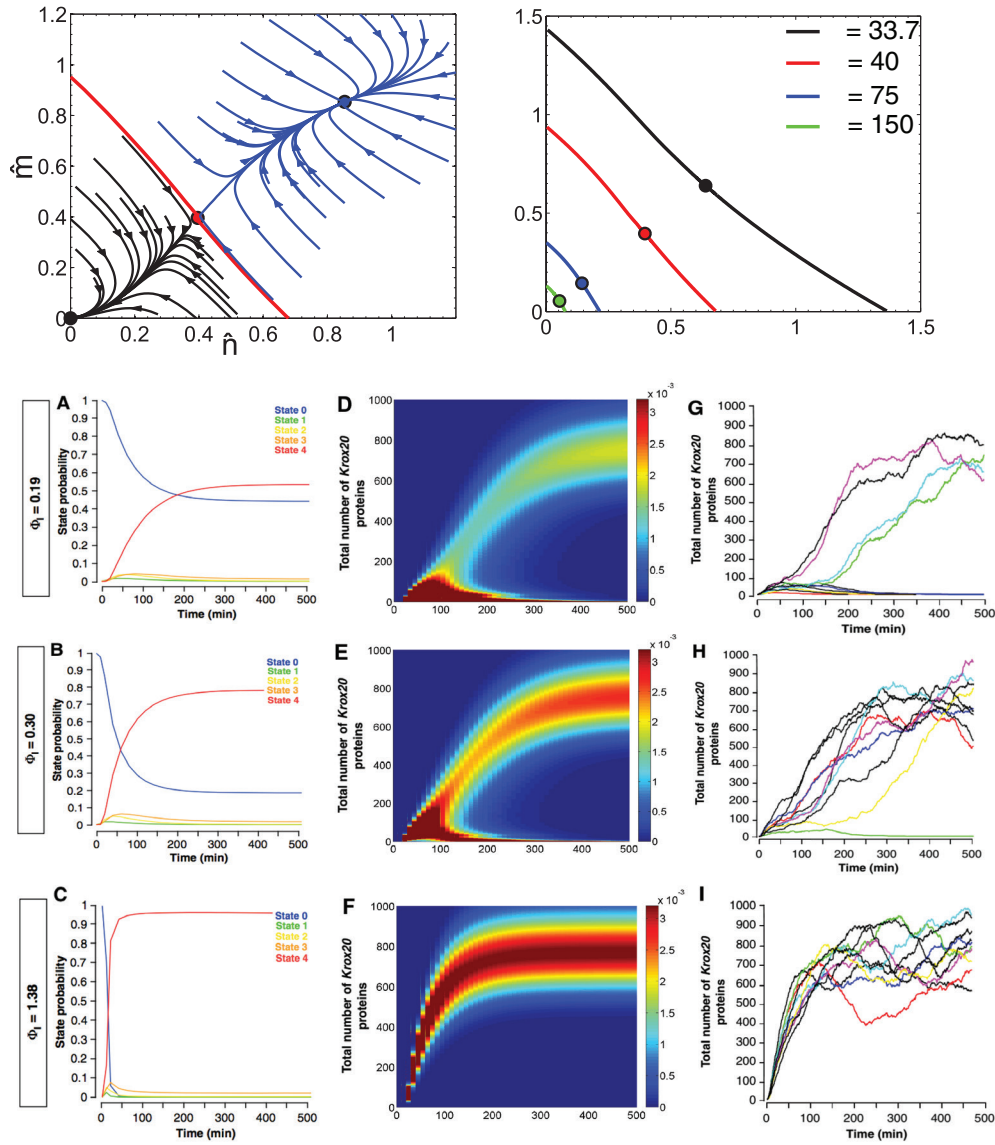
Figure 9. Mean-field modeling of protein activation Upper: Left, Phase-space analysis. Fixed points of the deterministic system. For $\alpha > \alpha_{\min} \approx 33.8$, the two attractors are characterized by two stable fixed points (black and blue) and a saddle point (red) located on the separatrix. Blue trajectories converge to the high expression level, whereas low proteins expression is found in the other basin of attraction (black trajectories), separated by a separatrix (red curve). Right: the separatrix is shown for various values of α. The basin of attraction of the fixed point $\hat{m}^* = \hat{n}^* = 0$ shrinks with increasing α. Lower pannel ((A)–(C)) Time-dependent probability of the different states of element A (s = 0, 1, 2, 3 or 4), for three different levels of initiation. ((D)–(F)) Evolution of the probability distribution for the number of proteins with initiation as in ((A)–(C)). Insets are magnification for protein numbers. ((G)–(I)) Stochastic simulations for the number of proteins. Results in panels (A)–(F) were obtained by integrating the Master equation. The molecular dynamics simulations in (G)–(I) are obtained from the Master equation, using the Gillespie algorithm [85].

10. General conclusion and perspective

We reviewed here the influential Smoluchowski equation and its applications in modeling, analysis in biophysics and computational cell biology. In general stochastic processes have now become the framework for extracting features from molecular and cellular large data sets. In that context, the Narrow Escape Theory is a coarse-graining procedure revealing how structures (geometry) controls physiology through time scales and rare random events. The Smoluchowski equation is also the basis for analysis super-resolution data and obtained deconvolution algorithms for extracting biophysical parameters [56]. The analysis of diffusion with obstacles reveals how narrow passage between obstacles defines the effective measured diffusion.

Polymer models allow computing looping rates used to interpret large data about the position of chromosomes inside the cell nucleus. We also illustrated stochastic processes in system biology by presenting a stochastic model that couples continuum and discrete levels. Stochastic gene activation, mRNA and protein productions remain an exciting field where the model analysis remains difficult due to the large degree of freedom (large parameter space). A general framework to extract parameters and study feedback loop in gene activation is still to be found.

Although stochastic chemical reactions are now routinely simulated using the classical Gillespie's algorithm, exploring the parameter space can be done when possible using asymptotic formulas, derived from the model equations. Another area that we have not reviewed here is the recent development of aggregation-dissociation with a finite number of particles. Smoluchowki fragmentation-aggregation model is an infinite set of equations that described colloids in solution and other molecular aggregations. However, aggregation with a finite number of particles to study viral capsid formation and telomere dynamics in the nucleus requires a different probability framework than infinite set of equations [82, 83], leading to novel quantity to estimate such as the time spent by two particles in the same cluster.

AQ3 AQ4 ## References

[1] Einstein A 1956 *Investigations on the Theory of the Brownian Movement* (New York: Dover) (translated and reprinted)
[2] Langevin P 1908 Sur la théorie du mouvement Brownien *C. R. Paris* **146** 530–3
[3] von Smolan Smoluchowski M R 1906 *Zarys Kinetycznej Teorji Ruchów Browna* vol A46 (Kraków: Akademii Umiejętności) pp 257–82
[4] von M Smoluchowski 1914 Studien über Molekularstatistik von Emulsionen und deren Zusammenhang mit der Brown'schen Bewegung *Wien. Ber.* **123** 2381–405
[5] Van Dyke M 1975 *Perturbation Methods in Fluid Mechanics* (Stanford, CA: The Parabolic Press)
[6] Wasow W 1986 *Linear Turning Point Theory* (New York: Springer)
[7] Bender C M and Orszag S A 1999 *Advanced Mathematical Methods for Scientists and Engineers. I. Asymptotic Methods and Perturbation Theory* (New York: Springer)
[8] Kevorkian J and Cole J D 1996 *Multiple Scale and Singular Perturbation Methods* (*Applied Mathematical Sciences* vol 114) (New York: Springer)
[9] Lagerstrom P A 1988 *Matched Asymptotic Expansions: Ideas and Techniques* (*Applied Mathematical Sciences* vol 76) (New York: Springer)
[10] Olver F J W 1974 *Asymptotics and Special Functions* (New York: Academic)
[11] Chandrasekhar S 1943 Stochastic problems in physics and astronomy *Rev. Mod. Phys.* **15** 2–89
[12] Kramers H A 1940 Brownian motion in field of force and diffusion model of chemical reaction *Physica* **7** 284–304
[13] Holcman D and Schuss Z 2016 Commentary: New mathematical physics needed for life sciences *Phys. Today* **69** 10

[14] Holcman D and Schuss Z 2015 *Stochatic Narrow Escape* (Berlin: Springer)
[15] Holcman D, Hoze N and Schuss Z 2011 Narrow escape through a funnel and effective diffusion on a crowded membrane *Phys. Rev.* E **84** 021906
Holcman D, Hoze N and Schuss Z 2012 *Phys. Rev.* E **85** 039903 (erratum)
[16] Schuss Z 1980 *Theory and Applications of Stochastic Differential Equations* (*Wiley Series in Probability and Statistics—Applied Probability and Statistics Section*) (New York: Wiley)
[17] Pontryagin L S, Andronov A A and Vitt A A 1933 On statistical considerations of dynamical systems *J. Exp. Theor. Phys.* **3** 165–80
[18] Schuss Z 2010 *Theory and Applications of Stochastic Processes: an Analytical Approach* (*Applied Mathematical Sciences* vol 170) (New York: Springer)
[19] Karlin S and Taylor H M 1981 *A Second Course on Stochastic Processes* (New York: Academic)
[20] John James Waterston, a neglected pioneer of the kinetic theory of gases https://en.wikipedia.org/wiki/John_James_Waterston
[21] Perrin J 1908 L'agitation moléculaire et le mouvement Brownien *C. R. Paris* **146** 967–70
[22] Svedberg T 1906 Über die Eigenbewegung der Teilchen in kolloidalen Lösungen I *Z. Elektrochem. Angew. Phys. Chem.* **12** 853–60
[23] Svedberg T 1910 Nachweis der von der kinetischen Theorie Geforderten Bewegung gelöster Moleküle *Z. Phys. Chem.* **74** 738
[24] Westgren A 1916 Die Veranderungsgeschwindigkeit der lokalen Teilchenkonzentration in Kolloiden Systemen, I *Ark. Mat. Astron. Fys.* **11** 1–24
[25] Westgren A 1918 Die Veranderungsgeschwindigkeit der lokalen Teilchenkonzentration in Kolloiden Systemen, II *Ark. Mat. Astron. Fys.* **13** 1–18
[26] Sutherland W 1905 A dynamical theory of diffusion for non-electrolytes and the molecular mass of albumin *Phil. Mag.* **9** 781–5
[27] Paley R N, Wiener N and Zygmund A 1933 Note on random functions *Math. Z.* **37** 647–68
[28] Lévy P 1954 *Le Mouvement Brownien* (*Mémorial des Sciences Mathématiques* vol 76) (Paris: Société Mathématique de France)
[29] Itô K 1944 Stochastic Integral *Proc. Imp. Acad.* **20** 519–24
[30] Feller W 1968 *An Introduction to Probability Theory and its Applications* vol I and II, 3rd edn (New York: Wiley)
[31] Landauer R 1983 *Self-Organizing Systems: the Emergence of Order* ed F E Yates *et al* (New York: Plenum)
[32] Hänggi P, Talkner P and Borkovec M 1990 50 years after Kramers *Rev. Mod. Phys.* **62** 251–341
[33] Hille B 2001 *Ionic Channels of Excitable Membranes* 3rd edn (Sunderland, MA: Sinauer)
[34] Eisenberg R S 1999 From structure to function in open ionic channels *J. Membr. Biol.* **171** 1–24
[35] Ward M J and Keller J B 1993 Strong localized perturbations of eigenvalue problems *SIAM J. Appl. Math.* **53** 770–98
[36] Ward M J, Henshaw W D and Keller J B 1993 Summing logarithmic expansions for singularly perturbed eigenvalue problems *SIAM J. Appl. Math.* **53** 799–828
[37] DiMarzio E and Mandell J A 1997 Phase transition behavior of a linear macromolecule threading membrane *Chem. Phys.* **107** 5510
[38] Holcman D and Schuss Z 2004 Escape through a small opening: receptor trafficking in a synaptic membrane *J. Stat. Phys.* **117** 191–230
[39] Schuss Z, Singer A and Holcman D 2007 The narrow escape problem for diffusion in cellular microdomains *Proc. Natl Acad. Sci. USA* **104** 16098–103
[40] Singer A, Schuss Z, Holcman D and Eisenberg R S 2006 Narrow escape, part I *J. Stat. Phys.* **122** 437–63
[41] Singer A, Schuss Z and Holcman D 2006 Narrow escape, part II: the circular disk *J. Stat. Phys.* **122** 465–89
[42] Singer A, Schuss Z and Holcman D 2006 Narrow escape, part III: non-smooth domains and Riemann surfaces *J. Stat. Phys.* **122** 491–509
[43] Singer A, Schuss Z and Holcman D 2011 Narrow escape and leakage of Brownian particles *Phys. Rev.* E **78** 051111
[44] Coombs D, Straube R and Ward M 2009 Diffusion on a sphere with localized traps: mean first passage time, eigenvalue asymptotics, and Fekete points *SIAM J. Appl. Math.* **70** 302–32
[45] Cheviakov A, Ward M J and Straube R 2010 An asymptotic analysis of the mean first passage time for narrow escape problems: part II: the sphere *SIAM Multiscale Model. Simul.* **8** 836–70

AQ5

[46] von Helmholtz H L F 1860 Theorie der Luftschwingungen in Röhren mit offenen Enden *Crelle Bn.* **57** 1–72

[47] Saxton M J 1995 Single-particle tracking: effects of corrals *Biophys. J.* **69** 389–98

[48] Saxton M J 2008 Single-particle tracking: connecting the dots *Nat Methods* **5** 671–2

[49] Manley S, Gillette J M, Patterson G H, Shroff H, Hess H F, Betzig E and Lippincott-Schwartz J 2008 High-density mapping of single molecule trajectories with photoactivated localization microscopy *Nat. Methods* **5** 155–7

[50] Sage D, Kirshner H, Pengo T, Stuurman N, Min J, Manley S and Unser M 2015 Quantitative evaluation of software packages for single-molecule localization microscopy *Nat Methods* **12** 717–24

[51] Giannone G *et al* 2010 Dynamic superresolution imaging of endogenous proteins on living cells at ultra-high density *Biophys. J.* **99** 1303–10

[52] Schneider R, Hosy E, Kohl J, Klueva J, Choquet D, Thomas U, Voigt A and Heine M 2015 Mobility of calcium channels in the presynaptic membrane *Neuron* **86** 672–9

[53] Brush S G 1976 The Kind of Motion We Call Heat: a History of the Kinetic Theory of Gases in the Nineteenth Century, Book 1: Physics and the Atomists. Book 2: Statistical Physics and Irreversible Processes

[54] Schuss Z 2011 *Nonlinear Filtering and Optimal Phase Tracking* (*Applied Mathematical Sciences* vol 180) (New York: Springer)

[55] Schuss Z 2013 *Brownian Dynamics at Boundaries and Interfaces In Physics, Chemistry, and Biology* (*Applied Mathematical Sciences* vol 186) (New York: Springer)

[56] Holcman D, Hoze N and Schuss Z 2015 Analysis and interpretation of superresolution single-particle trajectories *Biophys. J.* **109** 1761–71

[57] Hoze N, Nair D, Hosy E, Sieben C, Manley S, Herrmann A, Sibarita J B, Choquet D and Holcman D 2012 Heterogeneity of receptor trafficking and molecular interactions revealed by superresolution analysis of live cell imaging *Proc. Natl Acad. Sci. USA* **109** 17052–7

[58] Hoze N and Holcman D 2015 Recovering a stochastic process from super-resolution noisy ensembles of single-particle trajectories *Phys. Rev.* E **92** 052109

[59] Hoze N and Holcman D 2014 Residence times of receptors in dendritic spines analyzed by stochastic simulations in empirical domains *Biophys. J.* **107** 3008–17

[60] Holcman D and Schuss Z 2014 The narrow escape problem *SIAM Rev.* **56** 213–57

[61] Holcman D and Schuss Z 2014 Time scale of diffusion in molecular and cellular biology *J. Phys. A: Math. Theor.* **47** 173001

[62] Holcman D and Schuss Z 2013 Control of flux by narrow passages and hidden targets in cellular biology *Rep. Prog. Phys.* **76** 074601

[63] Holcman D and Schuss Z 2012 Brownian motion in dire straits *Multiscale Model. Simul.* **10** 1204–31

[64] Doi M and Edwards S F 1986 *The Theory of Polymer Dynamics* (Oxford: Oxford University Press)

[65] Kusumi A, Nakada C, Ritchie K, Murase K, Suzuki K, Murakoshi H, Kasai R S, Kondo J and Fujiwara T 2005 Paradigm shift of the plasma membrane concept from the two-dimensional continuum fluid to the partitioned fluid: high-speed single-molecule tracking of membrane molecules *Annu. Rev. Biophys. Biomol. Struct.* **34** 351–78

[66] Holcman D and Schuss Z 2011 Diffusion laws in dendritic spines *J. Math. Neurosci.* **1** 12041231

[67] Hoze N, Schuss Z and Holcman D 2013 Reconstruction of surface and stochastic dynamics from a planar projection of trajectories *SIAM J. Imaging Sci.* **6** 2430–49

[68] Min J, Holden S J, Carlini L, Unser M, Manley S and Ye J C 2014 3D high-density localization microscopy using hybrid astigmatic/ biplane imaging and sparse image reconstruction *Biomed. Opt. Express* **5** 3935–48

[69] Amitai A, Toulouze M, Dubrana K and Holcman D 2015 Analysis of single locus trajectories for extracting *in vivo* chromatin tethering interactions *PLoS Comput. Biol.* **11** e1004433

[70] Weiss G, Bendler J and Shlesinger M 1988 Polymer melt dynamics model with a relaxation time exponent of 10/3 *Macromolecules* **21** 521–3

[71] Chavel I and Feldman E A 1988 Spectra of Manifolds less a small domain *J. Duke Math.* **56** 399–414

[72] Abramowitz M and Stegun I 1972 *Handbook of Mathematical Functions with Formulas, Graphs, and Mathematical Tables* (New York: Dover)

[73] Amitai A, Kupka I and Holcman D 2012 *Phys. Rev. Lett.* **109** 108302

[74] Amitai A and Holcman D 2013 *Phys. Rev. Lett.* **110** 248105

J. Phys. A: Math. Theor. 00 (2016) 000000

Topical Review

[75] Xu Z, Duc K D, Holcman D and Teixeira M T 2013 The length of the shortest telomere as the major determinant of the onset of replicative senescence *Genetics* **194** 847–57

[76] Duc K D and Holcman D 2013 Computing the length of the shortest telomere in the nucleus *Phys. Rev. Lett.* **111** 228104

[77] ~~Backlund M P, Joyner R and Moerner W E 2015 Chromosomal locus tracking with proper accounting of static and dynamic errors *Phys. Rev.* E **91** 062716~~

[78] ~~Belopolskaya Ya I and Dalecky Yu L 2014 *Stochastic Equations and Differential Geometry* (Dordrecht: Springer)~~

[79] Knessl C, Matkowsky B, Schuss Z and Tier C 1985 An asymptotic theory of large deviations for markov jump-processes *SIAM J. Appl. Math.* **45** 1006–28

[80] Matkowsky B, Schuss Z, Knessl C, Tier C and Mangel M 1984 Asymptotic solution of the kramers-moyal equation and first-passage times for markov jump processes *Phys. Rev.* A **29** 3359–69

[81] Knessl C, Mangel M, Matkowsky B, Schuss Z and Tier C 1984 Solution of kramers-moyal equations for problems in chemical physics *J. Chem. Phys.* **81** 1285–93

[82] Hoze N and Holcman D 2013 Coagulation–fragmentation for a finite number of particles and application to telomere clustering in the yeast nucleus *Phys. Lett.* A **376** 845–9

[83] Hoze N and Holcman D 2015 Kinetics of aggregation with a finite number of particles and application to viral capsid assembly *J. Math. Biol.* **70** 1685–705

[84] Holcman D and Schuss Z A story of cellular time and the paradox of too many cell divisions prior to senescence (pre-print)

[85] Bouchoucha Y, Reingruber J, Le Men J, Gilardi-Hebenstreit P, Holcman D and Charnay P 2013 Stochastic switching in a feedback loop controls vertebrate hindbrain patterning revision *Mol. Syst. Biol.* **9** 690

[86] Reingruber J and Holcman D 2014 Computational and mathematical methods for morphogenetic gradient analysis, boundary formation and axonal targeting *Seminars in Cell & Developmental Biology* vol **35** (New York: Academic) pp 189–202